JOURNAL OF GEOPHYSICAL RESEARCH: OCEANS, VOL. 118, 2454–2475, doi:10.1002/jgrc.20166, 2013

Modeling Antarctic ice shelf responses to future climate changes and impacts on the ocean†

Kazuya Kusahara[1,2] and Hiroyasu Hasumi[1]

Received 18 January 2013; revised 14 March 2013; accepted 18 March 2013; published 14 May 2013.

[1] We investigate basal melting of all Antarctic ice shelves by a circumpolar ice shelf-sea ice-ocean coupled model and estimate the total basal melting of 770–944 Gt/yr under present-day climate conditions. We present a comparison of the basal melting with previous observational and modeling estimates for each ice shelf. Heat sources for basal melting are largely different among the ice shelves. Sensitivities of the basal melting to surface air warming and to enhanced westerly winds over the Antarctic Circumpolar Current are investigated from a series of numerical experiments. In this model the total basal melting strongly depends on the surface air warming but is hardly affected by the change of westerly winds. The magnitude of the basal melting response to the warming varies widely from one ice shelf to another. The largest response is found at ice shelves in the Bellingshausen Sea, followed by those in the Eastern Weddell Sea and the Indian sector. These increases of basal melting are caused by increases of Circumpolar Deep Water and/or Antarctic Surface Water into ice shelf cavities. By contrast, basal melting of ice shelves in the Ross and Weddell Seas is insensitive to the surface air warming, because even in the warming experiments there is high sea ice production at the front of the ice shelves that keeps the water temperature to the surface freezing point. Weakening of the thermohaline circulation driven by Antarctic dense water formation under warming climate conditions is enhanced by basal melting of ice shelves.

Citation: Kusahara, K., and H. Hasumi (2013), Modeling Antarctic ice shelf responses to future climate changes and impacts on the ocean, *J. Geophys. Res. Oceans*, *118*, 2454–2475, doi:10.1002/jgrc.20166.

1. Introduction

[2] Ice shelves are marine termini of ice sheets and are afloat in the ocean. Greenland and Antarctica have ice shelves in their coastal margins. There are many ice shelves around the Antarctic continent. The Antarctic ice shelves constitute 11% of all Antarctic Ice Sheet in the areal extent and enclose 44% of the coastline [*Drewry et al.*, 1982; *Fox and Cooper*, 1994]. There are two processes, iceberg calving at ice shelf fronts and basal melting/freezing, which induce mass exchange between ice sheet and ocean. These two processes are the main ablation mechanisms in the total mass balance over the Antarctic Ice Sheet. Although there are other ablation processes, such as runoff from surface melting of ice sheets, horizontal snow transport, and blowing-snow sublimation, these components are considered to be small. Mass exchange between the Antarctic Ice Sheet and the Southern Ocean has drawn much attention scientifically and societally, because it directly results in global sea level change [*Rowley et al.*, 2007; *Li et al.*, 2009]. Melting of icebergs and ice shelves by itself contributes little to the sea level change [*Jenkins and Holland*, 2007], because they are already afloat in the ocean. However, a change of the shape of ice shelf by collapse or basal melting could alter stress distribution of the ice shelf. Subsequently the information could be rapidly transmitted to the ice sheet interior through ice sheet dynamics [*Schoof*, 2007], and could be a trigger for an abrupt change of ice sheets and sea level.

[3] Recent satellite analyses show a significant increase of ice discharges from the Antarctic Ice Sheet, in particular from small ice shelves in the Amundsen Sea Embayment, suggesting a negative mass balance of the Antarctic Ice Sheet [*Rignot et al.*, 2008, 2011]. Thinning of the ice sheet interior near coastal regions has been observed [*Rignot et al.*, 2008; *Pritchard et al.*, 2009; *Wingham et al.*, 2009], and its main cause is considered to be interactions between ice shelf and ocean [*Rignot and Jacobs*, 2002; *Payne et al.*, 2007; *Jacobs et al.*, 2011; *Pritchard et al.*, 2012].

[4] Temperature and salinity in the Southern Ocean have also changed significantly in recent decades [*Gille*, 2002; *Levitus et al.*, 2005; *Boyer et al.*, 2005]. Mass losses from the Antarctic ice shelves result in additional freshwater flux into

† This article was originally published online on 14 May 2013. An error was subsequently identified. Figure 5 in the original version of this article was incorrect and has been updated on 18 May 2013.

[1] Atmosphere and Ocean Research Institute, The University of Tokyo, Chiba, Japan.

[2] Now at Institute of Low Temperature Science, Hokkaido University, Sapporo, Japan.

Corresponding author: K. Kusahara, Institute of Low Temperature Science, Hokkaido University, N19W8, Kita-ku, Sapporo 060-0819, Japan. (kazuya.kusahara@lowtem.hokudai.ac.jp)

©2013. American Geophysical Union. All Rights Reserved.
2169-9275/13/10.1002/jgrc.20166

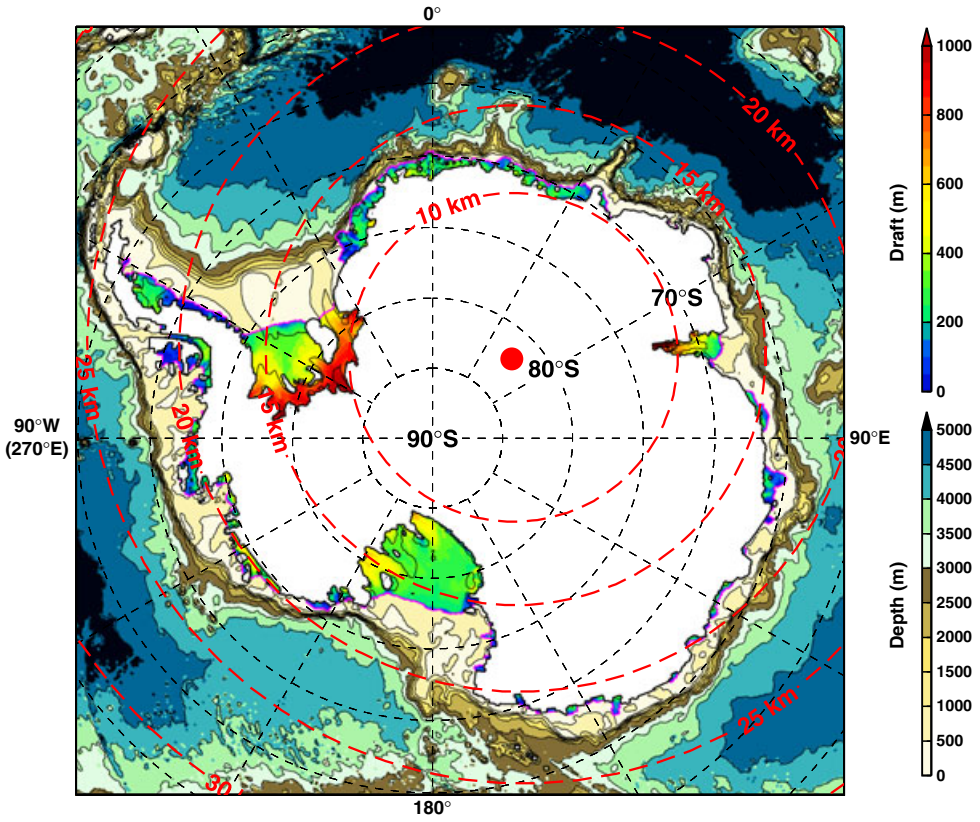


Figure 1. Bottom topography (color and contour) and ice shelf draft (color) in the model. Horizontal grid spacing is shown by red dashed contours. A red dot indicates one of the two singular points of the horizontal curvilinear coordinate.

the ocean. In particular, basal melting of ice shelves can be considered to have a large impact on dense water formation processes, because high sea ice production areas, such as coastal polynyas, are often located next to ice shelves. Over the recent decades, freshening of the Antarctic Bottom Water (AABW) in the Ross Sea has been observed [*Jacobs et al.*, 2002; *Jacobs*, 2004; *Jacobs and Giulivi*, 2010]. It has been suggested from ocean observations that enhanced melting of the continental ices in the Amundsen Sea Embayment contributes to the freshening of the AABW in the Ross Sea [*Hellmer and Jacobs*, 1994; *Shepherd et al.*, 2004; *Jacobs and Giulivi*, 2010]. Moreover, the freshening trend in the Ross Sea is considered to propagate downstream, indicating that the local changes of the ice shelves and the ocean in the Ross and Amundsen Seas have impacts on water properties in the remote Australian-Antarctic Basin [*Aoki et al.*, 2005; *Rintoul*, 2007; *Shimada et al.*, 2012].

[5] IPCC climate models project a continuous warming trend of the Antarctic atmospheric temperature over the 21st century [*Bracegirdle et al.*, 2008]. These climate models also project a subsurface ocean warming around the Antarctic continent [*Yin et al.*, 2011]. These results could indicate enhanced melting of ice shelves in the future and a large increase of mass loss from the Antarctic Ice Sheet. However, since these climate models do not have any ice shelf component in their model frameworks, it is difficult to assess quantitatively how much the melting of ice shelves increase in the future.

[6] In ocean general circulation models, an ice front between ice shelf and ocean had been often treated as a solid continental boundary. Over the past decade, three-dimensional ocean models which include an elaborate ice shelf component have been developed, and the ice shelf-ocean interaction and their impact on sea ice and ocean have been investigated [*Assmann et al.*, 2003; *Assmann and Timmermann*, 2005; *Beckmann et al.*, 1999; *Holland et al.*, 2010; *Jenkins and Holland*, 2002; *Losch*, 2008; *Makinson et al.*, 2011, *Reddy et al.*, 2010; *Thoma et al.*, 2006, 2008, 2010; *Timmermann et al.*, 2002a, 2002b; *Williams et al.*, 1998, 2002; *Galton-Fenzi et al.*, 2012]. However, most of the previous ice shelf-ocean modeling studies use regional models in which a few ice shelves are represented in the model domain. The regional modeling successfully reproduced local processes of the ice shelf ocean interaction in the model domain, but can not assess the impact of the processes on and from the ocean outside of the domain. Although there are a few studies which use circumpolar-domain models, they only represent large ice shelves due to the coarse horizontal resolution [*Hellmer*, 2004; *Losch*, 2008]. These coarse horizontal resolution models can not assess the impact of all Antarctic ice shelves on the Southern Ocean.

[7] As mentioned above, large changes are observed at small ice shelves. Therefore, a higher horizontal resolution model which can resolve all Antarctic ice shelves is required to better understand the Southern Ocean, and such mod-

Table 1. List of Numerical Experiments and Results of Total Basal Melting Amount, Sea Ice Production in Coastal Area, and Magnitude of the AABW Cell

Name	Description	Total Melt[a] (Gt/yr)	Ice Production[b] ($\times 10^3$km^3/yr)	AABW Cell[c] (Sv)
CTRL	Control case	769.6	25.1	–12.4
CTEMP1	+1°C south of 60°S	809.9	23.8	–11.8
CTEMP2	+2°C south of 60°S	892.8	22.7	–11.0
CTEMP3	+3°C south of 60°S	978.5	21.7	–10.1
CTEMP4	+4°C south of 60°S	1112.4	20.7	–9.2
CTEMP5	+5°C south of 60°S	1225.5	19.8	–7.8
CTEMP6	+6°C south of 60°S	1370.5	18.9	–6.4
TAUX4	$+0.04\text{Pa} \times \exp\left[-\left(\frac{\phi+55}{5}\right)^2\right]$	770.4	24.8	–12.6
TAUX8	$+0.08\text{Pa} \times \exp\left[-\left(\frac{\phi+55}{5}\right)^2\right]$	769.6	24.5	–12.8
NOTHM	No thermodynamic interaction under ice shelf	–	24.4	-13.6
NOTHM1	+1°C south of 60°S	–	23.2	–12.9
NOTHM2	+2°C south of 60°S	–	22.0	–12.5
NOTHM3	+3°C south of 60°S	–	21.0	–12.0
NOTHM4	+4°C south of 60°S	–	20.1	–11.4
NOTHM5	+5°C south of 60°S	–	19.1	–11.0
NOTHM6	+6°C south of 60°S	–	18.3	–10.0

[a]The total melting amount is calculated from freshwater flux with an assumption of a sea water density of 1028 kg m^{-3}.

[b]The ice production is calculated by the sum of daily sea ice formation rate over the Antarctic coastal region within 120 km from coastline or ice front (see a green line in Figure 3a).

[c]The magnitude of the AABW Cell is calculated by averaging stream function over the density range of 27.84–27.90 kg m^{-3} and the latitude range of 70°S and 64°S (see the pink box in Figure 13).

eling efforts are already in progress [*Galton-Fenzi*, 2010; *Hellmer et al.*, 2012; *Timmermann et al.*, 2012]. However, until now, the number of studies whose models resolve all Antarctic ice shelves in the circumpolar domain is very limited and thus characteristics and impact of all ice shelves around Antarctica are not clearly understood.

[8] In this study we aim to estimate basal melting of all ice shelves by an ice shelf-sea ice-ocean coupled model. The model horizontal resolution in Antarctic coastal margins is 10–20 km, therefore, we represent almost all Antarctic ice shelves in a single model. However, small ice shelves, such as Pine Island Glacier, are only marginally resolved. It should also be noted that the current model resolution is insufficient to resolve oceanic mesoscale eddies. Next, we investigate the response of ice shelves to possible future climate changes and their impact on ocean.

2. Numerical Model and Experiments

2.1. Coupled Ice Shelf-Sea Ice-Ocean GCM

[9] We use a sea ice-ocean coupled model, named COCO [*Hasumi*, 2006], and incorporate an ice shelf component into the model, following *Losch* [2008]. The freshwater flux at ice shelf bases is calculated with a three-equation scheme, based on a pressure-depending freezing point equation and conservation equations of heat and salinity [*Holland and Jenkins*, 1999]. Constant coefficients are used for thermal and salinity exchange velocities ($\gamma_t = 1.0 \times 10^{-4}$ ms^{-1}, $\gamma_s = 5.05 \times 10^{-7}$ ms^{-1}) [*Hellmer and Olbers*, 1989]. This parameter set is often used for a velocity-independent parameterization of ice shelf-ocean interaction [*Beckmann et al.*, 1999; *Timmermann et al.*, 2002a; *Dinniman et al.*, 2007; *Losch*, 2008; *Heimbach and Losch*, 2012]. The calculated freshwater flux and the associated heat flux are imposed on the ice shelf-ocean interface.

[10] The sea ice and ocean components of this model are similar to those described by *Kusahara et al.* [2010] and *Kusahara et al.* [2011]. High horizontal resolution models which resolve coastal topographic features enable us to simulate high sea ice production and dense water formation in Antarctic coastal margins [*Marsland et al.*, 2004; *Kusahara et al.*, 2010, 2011]. Note that the model used in

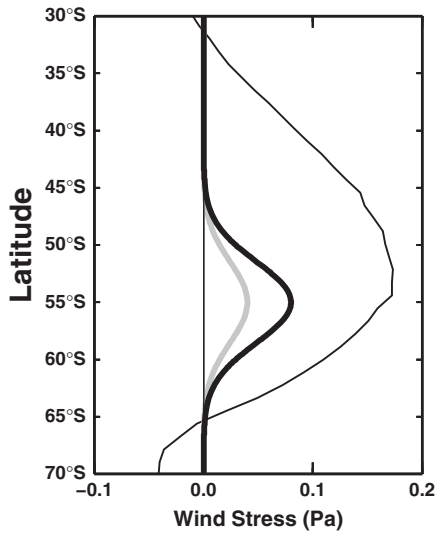


Figure 2. Zonal, annual mean wind stress distribution (thin line) and anomalies of wind stress for the TAUX4 (gray line) and TAUX8 (thick line) cases.

this study can also reproduce Antarctic coastal polynyas and high sea ice production there. Only the major differences from the previous model of *Kusahara et al.* [2011] are described here. The vertical coordinate system of the ocean model is a hybrid of σ (normalized depth) and z. There are 89 vertical levels: σ coordinate is applied to the four uppermost levels between the free surface and 40 m below the mean surface level, and the z coordinate is applied below. The ice shelf component is only applied to the z-coordinate domain. The vertical grid spacing in the z-coordinate region is 40 m (49 grids) above 2000 and 100 m (36 grids) below 2000 m. A partial step representation is adopted for both the bottom topography and ice shelf draft to better represent them in a z-coordinate ocean model [*Adcroft et al.*, 1997; *Losch*, 2008].

[11] The ocean model includes the uniformly third order polynomial interpolation algorithm for tracer advection [*Leonard et al.*, 1993], isopycnal diffusion, isopycnal layer thickness diffusion [*Gent et al.*, 1995], and a surface mixed layer parameterization based on turbulence closure [*Noh and Kim*, 1999]. The isopycnal diffusion coefficient is 1.0×10^{1} m^2s^{-1} and the thickness diffusion coefficient is 1.0 m^2s^{-1}. The background vertical diffusion coefficient is 2.0×10^{-5} m^2s^{-1}. The background vertical viscosity coefficient is 1.0×10^{-4} m^2s^{-1}. Under ice shelves, the surface mixed layer parameterization is turned off. Horizontal eddy viscosity is parameterized by a Laplacian form, and its coefficient spatially varies so as to resolve the Munk layer. The friction on solid boundaries (ocean floor and ice shelf base) is parameterized by a simple quadratic law with a constant drag coefficient of 1.3×10^{-3}. Unstable stratification in this model is removed by a simple convective adjustment scheme.

[12] Model bathymetry, coastline/icefront and ice shelf draft are shown in Figure 1. The model domain is taken to be the entire Southern Ocean and the northern boundary is placed at about 35°S. The bathymetry and ice shelf draft are derived from the RTopo-1 data set [*Timmermann et al.*, 2010]. A singular point of horizontal curvilinear coordinate is placed in the region south of the Amery Ice Shelf (45.0°E, 82°S, a red dot in Figure 1) to evenly resolve Antarctic coastal margins. The other singular point is placed on the north pole. By this grid configuration, the horizontal grid spacing over Antarctic coastal regions is between 10 and 20 km.

[13] Initial values for temperature and salinity fields are derived from Polar Science Center Hydrographic Climatology (PHC) [*Steele et al.*, 2001] and those for the ocean velocities are set to zero. In the northern six grids, temperature and salinity are restored to the PHC monthly mean climatology throughout the water column with a damping time scale of 10 days. To drive the model, we use the daily surface atmospheric climatology of *Röske* [2006], which is based on ECMWF Re-Analyses (ERA). This numerical experiment is hereinafter referred to as CTRL case. A 25 year simulation of the CTRL case is performed. It should be noted that after about 15 year integration, modeled basal melting reaches a quasi steady state.

[14] Additionally, we perform a simulation for the period from 1979 to 2011 with surface boundary conditions calculated from daily ERA-Interim data set [*Dee et al.*, 2011]. This numerical experiment is hereinafter referred to as ERA-INT case. To avoid an initial shock to the modeled system caused by changing the surface boundary conditions, the initial fields for this experiment is calculated by integrating the model for 6 years under the 1979 forcing data and starting from the quasi steady state of the CTRL case.

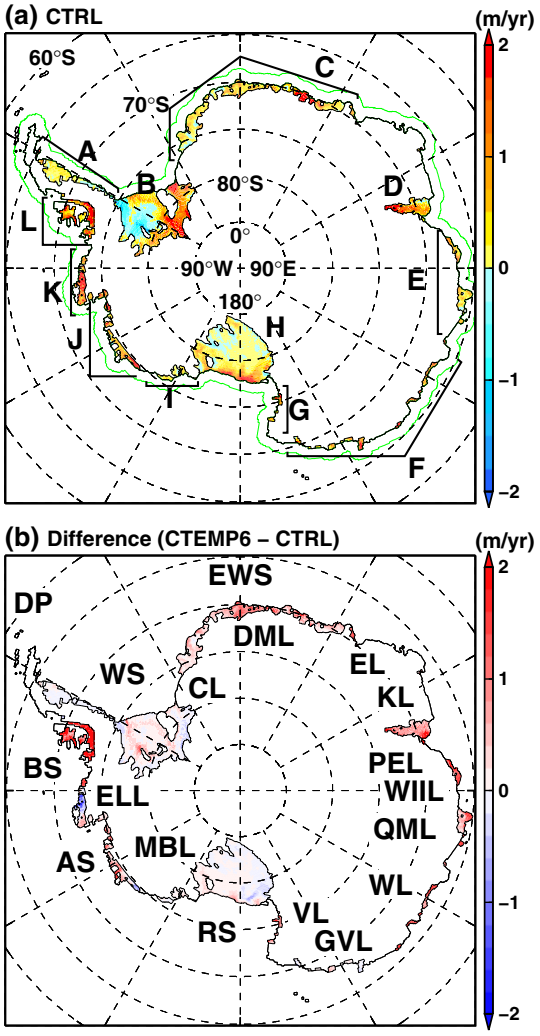


Figure 3. Spatial distribution of (a) annual basal melting/freezing rate (m/yr) in the CTRL case and (b) the anomaly of the melting/freezing rate in the CTEMP6 case from that in the CTRL case. In Figure 3a, positive values indicate melting. Labels A–M are used for Table 2. Green line in Figure 3a shows 120 km distance from coastline or ice front. In Figure 3b, DP indicates Drake Passage; WS, Weddell Sea; EWS, Eastern Weddell Sea; CL, Coats Land; DML, Dronning Maud Land; EL, Enderby Land; KL, Kemp Land; PEL, Princess Elizabeth Land; WIIL, Wilhelm II Land; QML, Queen Mary Land; WL, Wilkes Land; GVL, George V Land; VL, Victoria Land; RS, Ross Sea; MBL, Marie Byrd Land; AS, Amundsen Sea; ELL, Ellsworth Land; and BS, Bellingshausen Sea.

2.2. Sensitivity Experiments

[15] IPCC climate models commonly project a pronounced surface air warming trend all over the Southern Ocean and a continuous shift of the Southern Annular Mode (SAM) to more strongly positive states over the 21st century [*Fyfe and Saenko*, 2006; *Bracegirdle et al.*, 2008]. Along

Table 2. Results of Basal Melting Amount (BML) and the Corresponding Freshwater Flux (FWF) for 12 Categorized Ice Shelves (see Figure 3a for the Areas) in the CTRL, CTEMP6, and TAUX8 Cases

		This Study	CTRL		CTEMP6		TAUX8	
Ice Shelf	Ocean Sector	Area ($\times 10^3$km^2)	BML (Gt/yr)	FWF (mSv)	BML (Gt/yr)	FWF (mSv)	BML (Gt/yr)	FWF (mSv)
A		85.6	21.6	0.69	18.8	0.59	22.7	0.72
B	Atlantic Sector	438.1	160.5	5.09	193.6	6.14	159.4	5.06
C	(Weddell Sea)	223.8	107.6	3.41	251.2	7.96	108.4	3.44
D		68.1	70.3	2.23	127.5	4.04	73.5	2.33
E	Indian Sector	50.0	27.1	0.86	108.3	3.43	32.8	1.04
F		43.4	43.5	1.38	91.7	2.91	46.1	1.46
G		11.3	12.8	0.41	22.6	0.72	12.8	0.41
H	Ross Sea	479.8	110.7	3.51	119.0	3.77	110.4	3.50
I		23.3	4.8	0.15	6.0	0.19	4.8	0.15
J		61.8	58.7	1.86	88.2	2.80	59.2	1.88
K	Pacific Sector	42.3	68.6	2.17	78.3	2.48	70.2	2.23
L		71.2	83.3	2.64	265.3	8.41	69.3	2.20
TOTAL		1598.6	769.6	24.40	1370.5	43.46	769.6	24.40

with this SAM trend, an intensification and a poleward shift of the zonal wind stress are projected consistently among the models [*Fyfe and Saenko*, 2006]. Other atmospheric conditions, such as precipitation, downward radiation, and coastal winds could change largely in the future and have some impact on basal melting of ice shelves. However, there is no consensus on changes of these components at this time. In this study, we investigate the response of basal melting of Antarctic ice shelves to surface air warming and stronger westerly winds, which are most likely to occur in the next 100 years. For this purpose, we perform a series of numerical experiments driven by ideally modified surface forcings, as described below.

[16] The setup of the numerical experiments is summarized in Table 1. Anomalies from +1°C to +6°C are superimposed on the surface air temperature uniformly south of 60°S (CTEMP1, CTEMP2, CTEMP3, CTEMP4, CTEMP5, and CTEMP6 cases). Zonal wind stress anomalies with the amplitude of +0.04 and +0.08 Pa are superimposed on surface zonal wind stress uniformly (TAUX4 and TAUX8 cases). The shape of the zonal wind stress anomalies is given by a standard normal distribution (Table 1 and Figure 2). The meridional extent to which the zonal wind stress anomalies are applied is smaller than that estimated in *Fyfe and Saenko* [2006] in order not to modify coastal wind stresses. This treatment is done to selectively enhance the driving force over the Antarctic Circumpolar Current region without largely changing coastal sea ice fields. Numerical experiments without the thermodynamic interaction under ice shelf are also performed to investigate the impact of melt water from ice shelves on the ocean (NOTHM, NOTHM1, NOTHM2, NOTHM3, NOTHM4, NOTHM5, and NOTHM6 cases). The initial conditions for the NOTHM case is the same as those for the CTRL case, and the integration is also performed for 25 years. The initial condition for all the other experiments is taken from the end of year 15 in the CTRL/NOTHM case and a 10 year integration is performed for each case. After a few years, basal melting of ice shelves reaches a quasi-steady state and we use the model results for the last 5 years (21st–25th) for the analysis.

3. Results of the CTRL Case

3.1. Basal Melting/Freezing of Antarctic Ice Shelves

[17] In this section we show results of the CTRL case. Figure 3a shows a spatial distribution of basal melting/freezing of ice shelves around Antarctica (positive for melting). The distribution in the ERA-INT case is shown in Figures A1–A3 (see also Appendix A). For convenience of the quantitative comparison, we categorize the ice shelves into 12 groups based on the location (Figure 3a). All of the categorized ice shelves show net melting, and the total basal melting is 770 Gt/yr in the CTRL case and 944 Gt/yr in the ERA-INT case (Tables 2 and A1), which are consistent with

Table 3. Comparison With Previous Estimates of the Total Ice Shelf Basal Melting Amount for Antarctic Ice Shelves

Source	BML (Gt/yr)	Method
This study	770–944	circumpolar ice shelf-sea ice-ocean model
Timmermann et al. [2012]	1600	circumpolar ice shelf-sea ice-ocean model
Hellmer [2004]	907	circumpolar ice shelf-sea ice-ocean model
Rignot and Jacobs [2008]	1030	remote sensing
Jacobs et al. [1996]	756±380	composite of observation and modeling

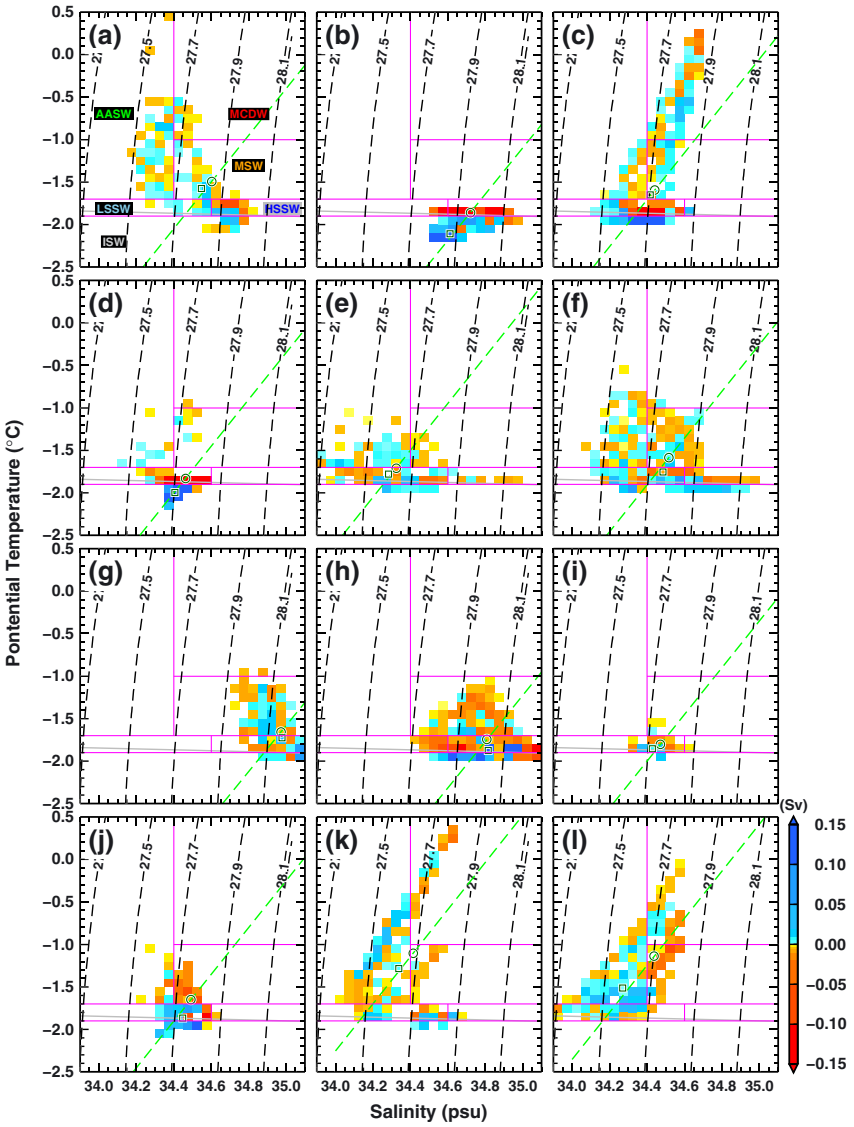


Figure 4. Water exchange across ice front in potential temperature-salinity space. Bin intervals for potential temperature (the vertical axis) and salinity (the horizontal axis) are 0.1°C and 0.05 psu. Blue and red colors indicate outflow from the cavity and inflow into the cavity, respectively. Green circle (square) indicates mean temperature and salinity for the inflowing (outflowing) water into (from) the ice shelf cavity. Green dashed line indicates a Gade line [*Gade*, 1979]. Pink lines indicate boundaries of water masses (Table 4). The abbreviations of the water masses are shown in Figure 4a. Gray line indicates the surface freezing temperatures. The dashed contours show the potential density anomaly.

previous estimates in observation-based and modeling studies (Table 3). Large areas of annual net freezing are found in the three largest ice shelves, i.e., the Filchner-Ronne, Amery, and Ross Ice Shelves and small patches of freezing areas are also found in other small ice shelves (A, C, E, I, and J). We show the detailed features of basal melting and comparisons with previous studies for each ice shelf in Appendix A. We consider that the model in this study can roughly reproduce the melting amount and the spatial melting distribution for Antarctic ice shelves under the present-day climate.

[18] The three largest ice shelves occupy 62% of the Antarctic ice shelf area. However, the melting amount in the three ice shelves accounts for only 44% of the total melting (Table 2). These results indicate that basal melting of the other small ice shelves, which are elongated along coast, is comparable to or larger than that of large ice shelves. This is consistent with a recent modeling study [*Timmermann et al.*, 2012].

3.2. Water Masses Into Ice Shelf Cavities

[19] Ocean heat melts the ice shelf base. There are three heat sources for basal melting [*Jacobs et al.*, 1992]. The first one is Shelf Water (SW), which originates from brine drainage by sea ice formation in winter. This water has near surface freezing temperatures. SW can melt ice shelf bases when it penetrates into ice shelf cavities because the freezing temperature of sea water decreases with depth. The second one is Circumpolar Deep Water (CDW), which is character-

Table 4. Definition of Water Masses Used in This Study[a]

	Water Mass	Temperature (°C)	Salinity (psu)
	AASW	$T \geq -1.7$	$S < 34.4$
CDW	MCDW	$T \geq -1.0$	$S \geq 34.4$
	MSW	$-1.7 \leq T < -1.0$	$S \geq 34.4$
SW	LSSW	$-1.9 \leq T < -1.7$	$S < 34.6$
	HSSW	$-1.9 \leq T < -1.7$	$S \geq 34.6$
	ISW	$T < -1.9$	–

[a]AASW, Antarctic Surface Water; CDW, Circumpolar Deep Water; MCDW, Modified Circumpolar Deep Water; MSW, Modified Shelf Water; SW, Shelf Water; LSSW, Low Salinity Shelf Water; HSSW, High Salinity Shelf Water; and ISW, Ice Shelf Water.

ized by high temperature and high salinity. This water is a portion of the Antarctic Circumpolar Current at intermediate depths. A part of this water is observed to intrude into inner continental shelf regions through troughs and/or across sills at shelf breaks. During a journey towards the ice shelf, CDW is often converted to modified CDW (MCDW) by mixing with ambient waters. The temperature of MCDW is colder than that of the original CDW. The last one is warm Antarctic Surface Water (AASW). AASW is formed by sea ice melting and therefore is characterized by low salinities. During the summer sea ice-free period, AASW is warmed by surface heating, e.g., downward shortwave radiation. Warm AASW is transported to ice shelf cavities by tide and/or seasonally variable coastal currents, and melts ice shelf bases near ice front regions.

[20] We calculate volume transport of inflow and outflow across ice shelf fronts to investigate the heat sources for basal melting for each ice shelf. Figure 4 shows the inflow and outflow in the potential temperature-salinity space with bin intervals of 0.1°C and 0.05 psu. The characteristics of the inflow/outflow pattern is largely different among the ice shelves.

[21] We define water masses by potential temperature and salinity (Table 4), and calculate a ratio of each water mass volume to the total inflow into each ice shelf cavity (Figure 5). The water mass SW is divided into low salinity shelf water (LSSW) and high salinity shelf water (HSSW) by salinity. Modified Shelf Water (MSW) is a mixture of MCDW and SW. At ice shelves of West Antarctica (J, K, and L), CDW origin waters (MCDW and MSW) dominate the inflow. At the rest of the ice shelves, SW (LSSW and HSSW) dominates the inflow. CDW origin waters are found at all ice shelves except the Filchner-Ronne Ice Shelf (B). The warm ASSW is found at ice shelves of A, C, D, E, F, J, K, and L. The ice front of these ice shelves is exposed to coastal currents. These results indicate that the heat source for basal melting is largely different among ice shelves. Since ice shelves are melted by ocean and provide cold and fresh water in the ocean surface beneath the ice shelf, mean temperature and salinity of the outflow is colder and fresher than those of the inflow. It should be noted that the conversion of the temperature-salinity characteristics from the inflow to the outflow almost follows a Gade line [*Gade*, 1979], as shown by green dashed lines in Figure 4.

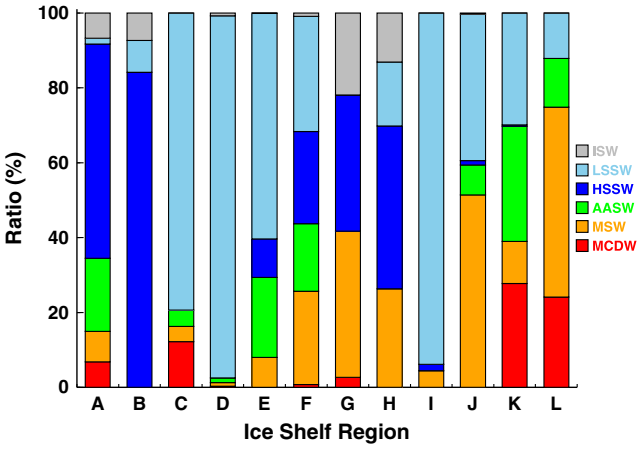


Figure 5. Ratio of water mass volumes to the total inflow into each ice shelf cavity. See Table 4 for the definition of water masses.

4. Response of Ice Shelf Basal Melting to Future Climate Changes

[22] In this section we show results of numerical experiments forced with possible future atmospheric conditions over the Southern Ocean (enhanced westerly winds and increased surface air temperatures). A summary of all the numerical experiments is listed in Table 1. In the TAUX4 and TAUX8 cases (Figure 2), the total melting amount, the melting/freezing pattern, and the feature of water mass exchange across ice fronts are almost the same as those in the CTRL case. This result indicates that, at least in this model, the enhanced westerly wind stresses over the Antarctic Circumpolar Current regions (Figure 2) hardly affects basal melting of the Antarctic ice shelves. Hereinafter, we show the results of numerical experiments for the surface air warming.

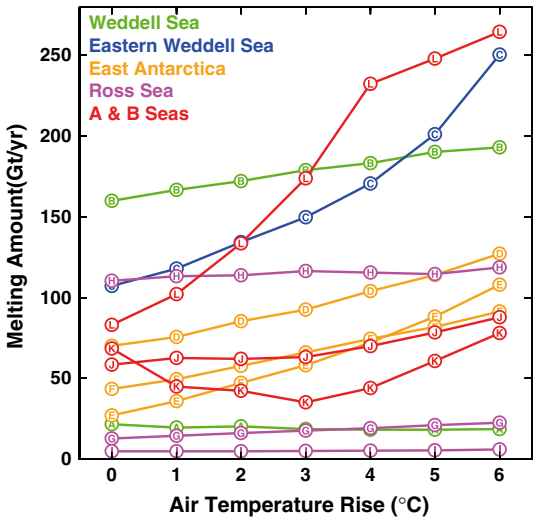


Figure 6. Response of basal melting of ice shelves to surface air warming.

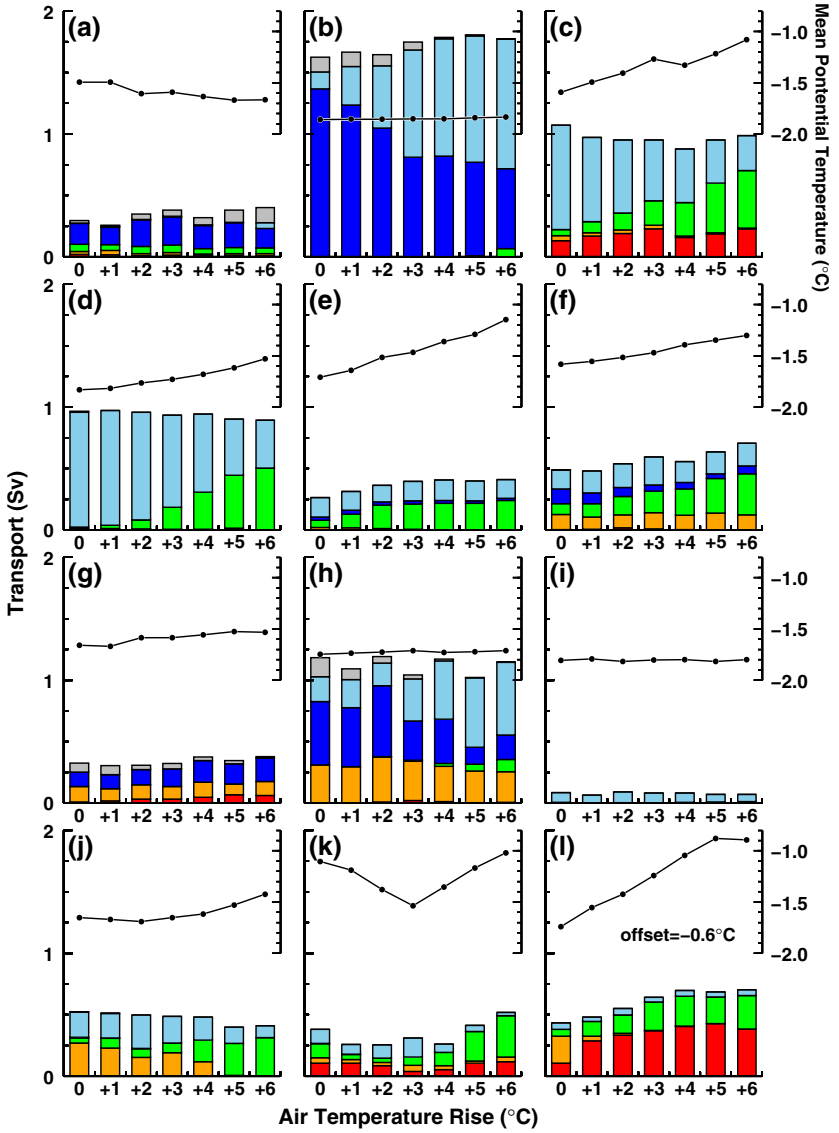


Figure 7. Volume transport of inflowing water masses into ice shelf cavities (the left axis) and the mean temperature of the inflow (the right axis) in the surface air warming experiments. Colors indicate water masses: red indicates MCDW, orange MSW, green AASW, blue HSSW, light blue LSSW, and gray ISW. See Table 4 for the definition of water masses. The mean temperature of the ice shelf L is shown with an offset of –0.6°C.

4.1. Sensitivity of Ice Shelf Basal Melting to the Surface Air Warming

[23] The total basal melting amount increases with the magnitude of the surface air warming (Table 1). Figure 3b shows a spatial distribution of anomalies of the basal melting rate in the CTEMP6 case from the CTRL case. Large positive anomalies are found on the most of ice shelves elongated along the Antarctic coast. On the other hand, there are no significant changes of the melting rate over the Filchner-Ronne and Ross Ice Shelves.

[24] The response of basal melting to the surface air warming significantly varies from one ice shelf to another, as shown in Figure 6. The largest response to the warming is found at the ice shelves in the western side of the Antarctic Peninsula (L). The basal melting amount increases from 83 to 265 Gt/yr. The second and third largest responses are found at the ice shelves in the Eastern Weddell Sea (C) and in the Indian sector (D, E, and F), respectively. The magnitude of the response of basal melting to the surface air warming is relatively small in the ice shelves in the Weddell Sea (A and B) and the Ross Sea (G, H, and I). In the ice shelves of K, the basal melting amount decreases in the 1–3°C surface air warming cases, and shifts to increase with surface air warming in the 4–6°C warming cases.

4.2. Changes of Water Masses Into Ice Shelf Cavities

[25] We investigate changes of water masses flowing into ice shelf cavities (Figure 7) to understand the response of ice shelf basal melting to the surface air warming (Figure 6). The response of ice shelf basal melting is explained by changes in the volume transport and the temperature of the inflow into ice shelf cavities (in other words, the heat

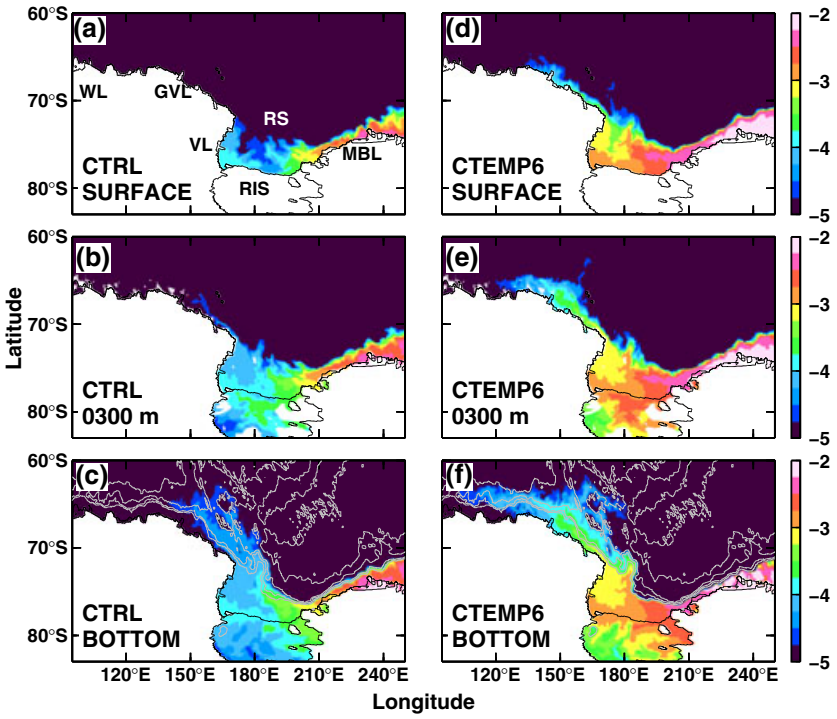


Figure 8. Spatial distribution of virtual tracer concentration at the surface, 300 m depth, and bottom in (a–c) the CTRL and (d–f) CTEMP6 cases. The tracer is released from the ice shelves in the Amundsen and Bellingshausen Seas (JKL). Gray contours in Figures 8c and 8f indicate bottom depth with 1000 m interval. A log10 scale is used for the tracer concentration. RIS indicates Ross Ice Shelf. The other abbreviations are the same as in Figure 3.

content of the inflow). This is naturally expected because we use constant thermal and salinity exchange velocities for solving the interaction between ice shelf and ocean. In the Filchner-Ronne and Ross Ice Shelves (B and H), the volume transport does not change significantly in all the surface air warming experiments when compared with that in the CTRL case, and the mean temperatures are kept at the near surface freezing temperatures. In these ice shelves, an increase of the LSSW component compensates the decrease of the HSSW one. The shift of the dominant water mass from HSSW to LSSW is due to a decrease of sea ice production at the front of these ice shelves and to an increase of basal melting of ice shelves in the upstream ice shelves, as discussed later.

[26] In the ice shelves in the Eastern Weddell Sea (C) and the Amery Ice Shelf (D), the main water mass into the ice shelf cavities is changed, although the inflow volume transport into the cavities does not change significantly. The LSSW component into the cavities decreases with the surface air warming and it is compensated by an increase of the warm AASW component. Since the temperature of AASW is higher than that of LSSW, the mean temperature of the inflow rises. Because the ice-covered period is shortened by surface air warming at the front of these ice shelves, warm AASW becomes to be easily formed in summer and to be transported into these ice shelf cavities. It should be noted that the inflows of AASW into cavities occur dominantly in late summer and fall. The existence of warm AASW under ice shelves is observed in the real ocean [*Hattermann et al.*, 2012]. The mechanisms of warm AASW in the surface intruding into the ice shelf cavities is considered to be an Ekman convergence at the ice fronts driven by westward wind stresses [*Ohshima et al.*, 1996]. In the ice shelves in the East Antarctica (E and F), the inflow of AASW increases along with air temperature rises, leading to raising the mean temperature and the inflow volume transport.

[27] In the ice shelves in the Amundsen Sea (J), the inflow volume transport of MSW decreases with the surface air warming, and the MSW component disappears in the 5–6°C surface air warming cases. The warm AASW component and the mean temperature into ice shelf cavities are increased. In the ice shelves in the western part of the Antarctic Peninsula (L), the inflow volume transport of MCDW and warm AASW are enhanced. In the Abbot Ice Shelf (K), the inflow volume transport of MCDW decreases with surface air warming below 3°C and that of the warm AASW increases with warming above 4°C. A part of the increased basal melt water from ice shelves K is advected to coastal regions at the front of ice shelves of L. The advected melt water stabilizes the water column there. The less dense water occupies the coastal regions and prohibits access of relatively dense MCDW to ice shelves of K.

5. Transport of Ice Shelf Basal Meltwater

5.1. Virtual Tracer Experiments

[28] The results of the previous section show that surface air warming over the Southern Ocean increases basal melting of ice shelves around Antarctica. The basal meltwater just off the ice shelves is advected by ambient ocean

currents, typically coastal currents, and could have some impact on ocean structure in remote basins. To investigate the behavior of ice shelf basal meltwater in detail, we perform virtual tracer experiments in which a tracer is released at the same rate as the basal meltwater of ice shelves and transported by modeled flows. We focus on the basal meltwater from the ice shelves in the Amundsen and Bellingshausen Seas (JKL) and in the Eastern Weddell Sea (C), since the response of these ice shelves to the surface air warming is very large (Figure 6). Two different virtual tracers are released from the ice shelves of JKL and C. No surface flux is imposed for the virtual tracers on the open ocean surface. This treatment is the same as that for chemical tracers which are released from ice shelf base [*Hellmer and Olbers*, 1989]. The virtual tracer experiment is performed for the CTRL and CTEMP6 cases. We perform a 10 year integration for each case, which starts from 1 January of 16th year. The initial condition tracer concentration is zero over the domain.

5.1.1. Basal Meltwater Tracer of Ice Shelves in the Amundsen and Bellingshausen Seas

[29] It is known that oceanic conditions in the Ross Sea are strongly influenced by variability in the Amundsen and Bellingshausen Seas through westward-flowing coastal currents [*Assmann and Timmermann*, 2005; *Jacobs and Giulivi*, 2010]. Figure 8 shows a spatial distribution of the virtual tracer that is released from ice shelves of JKL. It should be noted that we performed additional tracer experiments in which different virtual tracers are separately released from J, K, and L and found that all tracers are considerably advected to the continental shelf in the Ross Sea. Therefore, we describe the total behavior of the meltwater from JKL. Here, we show the concentration at the surface, 300 m depth, and the bottom at the end of the integration (December of the 25th year). Most of the virtual tracer released from ice shelves in the Amundsen and Bellingshausen Seas is advected eastward and toward lower latitudes by the Antarctic Circumpolar Current (not shown). A part of the tracer is advected westward/southwestward to the Ross Sea by the westward-flowing coastal current. The advected virtual tracer over the Ross Sea in the CTEMP6 case is much larger, by over one order of magnitude, than in the CTRL. For example, to the east of the Ross Ice Shelf, the surface tracer concentration is about 0.1×10^{-3} in the CTRL case and 3.0×10^{-3} in the CTEMP6 case. The salinity difference of the inflowing water mass into the cavity under the Ross Ice Shelf between the two cases is about 0.2 psu, and the dominant water mass into the cavity is changed from HSSW to LSSW (H in Figure 7). Basal meltwater of ice shelves from the Amundsen and Bellingshausen Seas explains half of the freshening and the rest is explained by the reduction of sea ice production at the front of the Ross Ice Shelf. The signal of increased basal meltwater extends to the inner part of cavity of the Ross Ice Shelf (Figures 8e and 8f).

[30] In the CTEMP6 case, a relatively high virtual tracer concentration extends to the Australian-Antarctic Basin at the mid depth and the bottom. The concentration at the bottom is higher than that at the mid depth. This suggests that meltwater advected from the Amundsen and Bellingshausen Seas to the Ross Sea penetrates into deep ocean at coastal polynyas in the Ross Sea. The spatial distribution of annual sea ice production in the CTRL case is shown in Figure 9a.

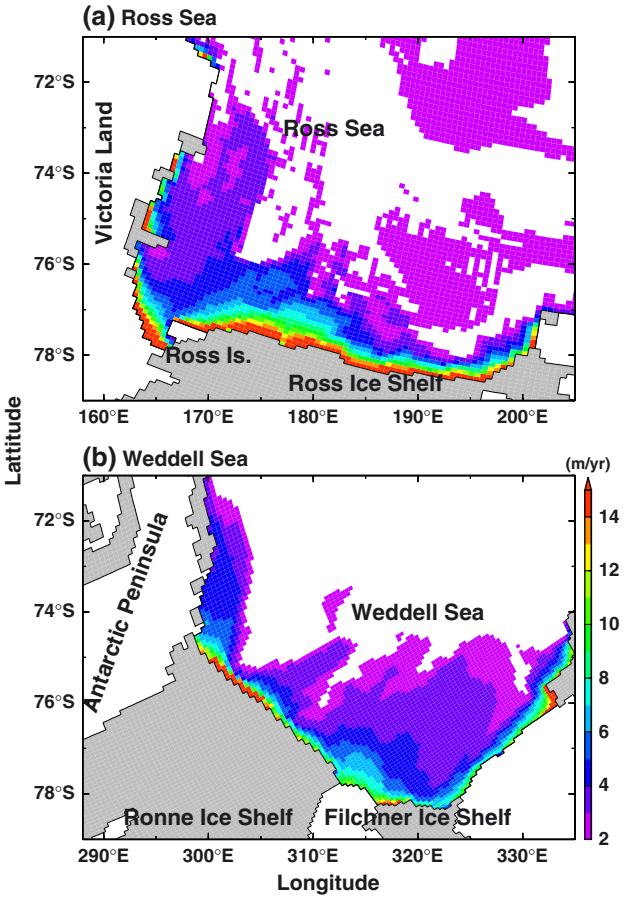


Figure 9. Spatial distribution of modeled annual sea ice production (m/yr) in the CTRL case. The area of net sea ice production smaller than 2 m/yr is masked out.

High sea ice production areas are found along ice front of the Ross Ice Shelf. This distribution is consistent with that estimated from satellite data and heat flux calculation [*Tamura et al.*, 2008; *Drucker et al.*, 2011], except McMurdo Sound (between Victoria Land and Ross Island), where the model overestimates sea ice production due to missing of fast ice. Although sea ice production in coastal areas is reduced in the CTEMP6 case, the magnitude is strong enough to drive a deep convection which mixes tracers from the surface to the bottom.

5.1.2. Basal Meltwater Tracer of Ice Shelves in the Eastern Weddell Sea

[31] It has been suggested that basal meltwater of the Eastern Weddell Ice Shelves have some impact on ocean structure in the Weddell Sea [*Thoma et al.*, 2010]. Figure 10 shows the spatial distribution of the virtual tracer that is released from ice shelves of C.

[32] In both cases, areas of high concentration are found on the southern and western continental slopes of the Weddell Sea. The virtual tracer concentration over the Weddell continental slope in the CTEMP6 case is more than threefold higher than that in the CTRL case. In the CTEMP6 case, the signal of basal meltwater of the Eastern Weddell Ice Shelves extends into the inner regions of the Filchner-Ronne Ice Shelf (Figures 10e and 10f). Similarly to the case of the

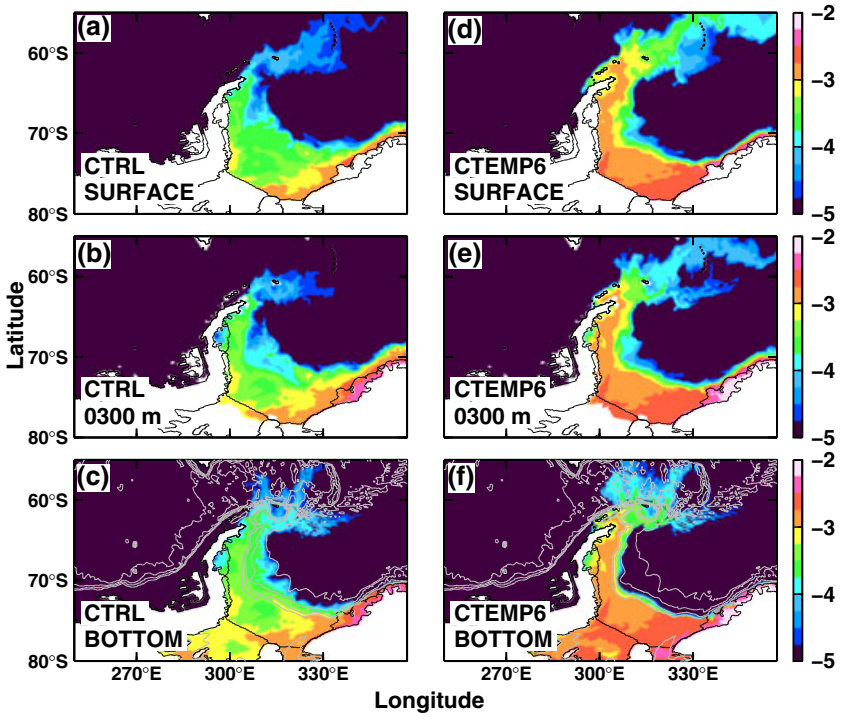


Figure 10. Same as Figure 8, but for the tracer released from the ice shelves in the Eastern Weddell Sea (C).

Ross Sea, there are high sea ice production areas at the front of the Filchner-Ronne Ice Shelf (Figure 9b) and thus the surface water containing the ice shelf basal meltwater can be transported to the bottom in winter.

5.2. Impact of Basal Meltwater on Deep Ocean

[33] As shown in the previous subsection, a part of the virtual tracers which mimics the basal meltwater from the ice shelves in the Amundsen and Bellingshausen Seas and the Eastern Weddell Sea is advected to the downstream regions. The tracers are transported to the bottom through high sea ice production in coastal areas. Here we investigate the impact of the meltwater on the deep-ocean water property. Figures 11 and 12 show anomalies of salinity in the CTEMP6 case from those in the CTRL case. The anomalies of the NOTHM6 case from the NOTHM case are also shown to separate the impact of increased meltwater on the water properties from the change of the water properties solely due to the surface air warming. It should be noted that surface air warming leads to a reduction of sea ice production in coastal margins (Table 1) and thus can also be a cause of freshening of bottom water.

[34] In the experiments with the ice shelf-ocean thermodynamic interaction, negative anomalies of salinity spread from the Ross Sea to the Australian-Antarctic Basin (Figure 11a), being consistent with the distribution of the virtual tracer (Figure 8). In particular, the pronounced negative salinity anomalies are found over the continental slope regions off the George V Land and Wilkes Land. In the experiments without the thermodynamic interaction, the signal weakens over the continental slope regions (Figure 11b). This result confirms that the increased meltwater from the ice shelves in the Amundsen and Bellingshausen Seas is a possible cause of freshening of the bottom water in the Australian-Antarctic Basin along with decrease of salt input by the surface air warming.

[35] A significant difference in the salinity anomalies is also found in the Weddell Sea between the cases with and without the thermodynamic interaction (Figure 12). The largest difference, about 0.02 psu, is found in the Powell Basin, in the northwestern Weddell Sea, and the signal spreads to the Scotia Sea through the Philip and South Orkney Passages. The location of the high salinity anomaly difference corresponds to the pathway of basal meltwater of the Eastern Weddell Ice Shelves (Figure 10).

6. Response of the Southern Ocean Meridional Overturning Circulation

[36] Figure 13 shows the stream function of zonally integrated, annual-mean meridional overturning circulation in the latitude-density domain for the CTRL case and its anomaly for the CTEMP6 case from the CTRL case. There is a deep cell with an absolute maximum value of 18.9 Sv in the bottom layer ($\sigma_0 > 27.80$ kg m^{-3}). The cell extends to lower latitudes. Since the deep cell is strongly related to the Antarctic Bottom Water formation in the Antarctic coastal regions [*Orsi et al.*, 1999; *Morales Maqueda et al.*, 2004], we call it hereinafter "the AABW cell". Under the 6°C warming case, the magnitude of the AABW cell is weakened by about 6 Sv (Table 1 and Figure 13b).

[37] Figure 14 shows the responses of the magnitude of the AABW cell to the surface air warming in the experiments with and without the thermodynamic interaction under ice shelf. Under the control surface boundary conditions, the magnitude of the AABW cell in the CTRL case is smaller

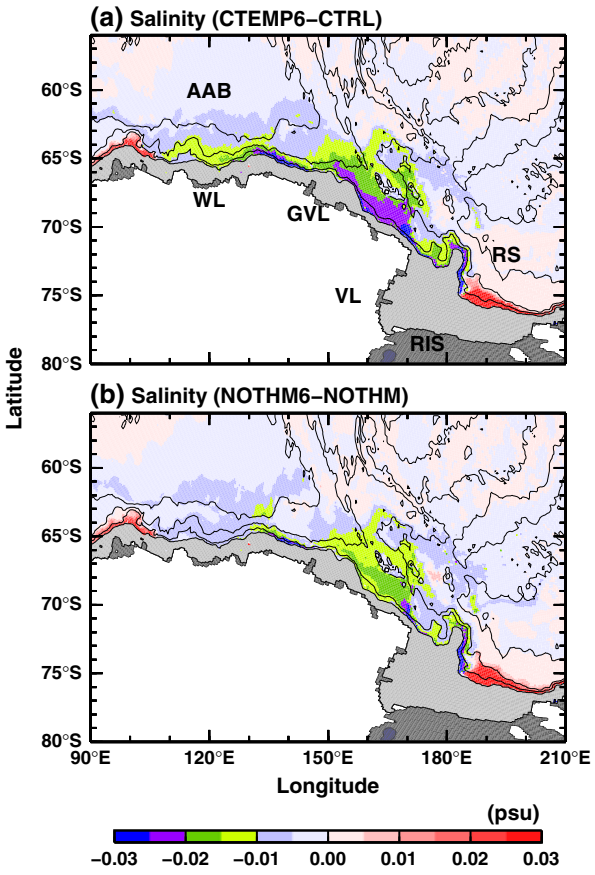


Figure 11. Spatial distribution of salinity anomalies at the bottom for the experiments with and without the thermodynamic interaction under ice shelf. Contours show bottom depth with 1000 m interval. The area where the sea floor is shallower than 1000 m is masked out by shade. AAB indicates Australian-Antarctic Basin, and RIS Ross Ice Shelf. The other abbreviations are the same as in Figure 3.

than that in the NOTHM case (Table 1), being consistent with a previous modeling study [*Hellmer*, 2004]. In both cases, the magnitude of the AABW cell tends to decrease with the surface air warming, because surface air warming reduces sea ice production in coastal areas (Table 1), which is a main driver of the AABW cell. However, the decreasing rate for the AABW cell in the experiments with the thermodynamic interaction is much larger than that without the thermodynamic interaction. About 48% reduction is found in the 6°C warming case in the experiment with the thermodynamic interaction (Table 1 and Figure 14). This result indicates that the response of ice shelves amplifies the weakening for the AABW cell under warming climate.

7. Summary and Discussion

[38] Using a circumpolar ice shelf-sea ice-ocean coupled model that resolves all ice shelves around Antarctica (Figure 1), we have investigated basal melting of the Antarctic ice shelves. We estimate the basal melting of the Antarctic ice shelves of 770–944 Gt/yr under present-day climate conditions. Ice discharge from the Antarctic Ice Sheet to the ocean is estimated to be in the range of 2000–2500 Gt/yr [*Rignot et al.*, 2008, 2011]. Assuming that basal melting of ice shelf accounts for 20%–40% of the total ice discharge [*Jacobs et al.*, 1992, 1996; *Hooke*, 2005], our model estimates are within a reasonable range (400–1000 Gt/yr). Moreover, our estimates are consistent with the previous observational and modeling estimates which ranges from 756 to 1600 Gt/yr (Table 3). It is also found that the model can roughly produce general basal melting/freezing patterns (Figures 3a and A1–A3). Only 44% of basal melting occurs at the three largest ice shelves and the rest does at the other small ice shelves. In terms of freshwater flux from the Antarctic ice shelves, this result strongly indicates the importance of basal melting of small ice shelves elongated along the coastline (Table 2). From investigations of water masses flowing into ice shelf cavities, it is found that heat sources for basal melting are largely different among the ice shelves (Figures 4 and 5).

[39] To show the response of basal melting of Antarctic ice shelves to future climate changes which are commonly projected in IPCC climate models [*Fyfe and Saenko*, 2006; *Bracegirdle et al.*, 2008], we have performed numerical experiments driven by possible future atmospheric conditions, in which surface air temperature in coastal regions

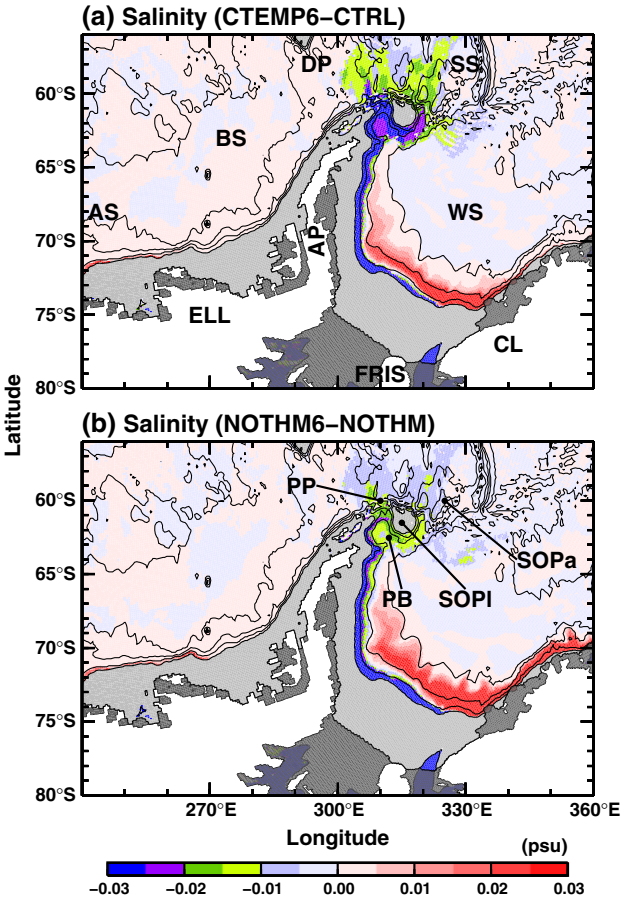


Figure 12. Same as Figure 11, but for the Bellingshausen and Weddell Seas. AP indicates Antarctic Peninsula, SS Scotia Sea, FRIS Filchner-Ronne Ice Shelf, PP Philip Passage, PB Powell Basin, SOPl South Orkney Plateau, and SOPa South Orkney Passage. The other abbreviations are the same as in Figure 3.

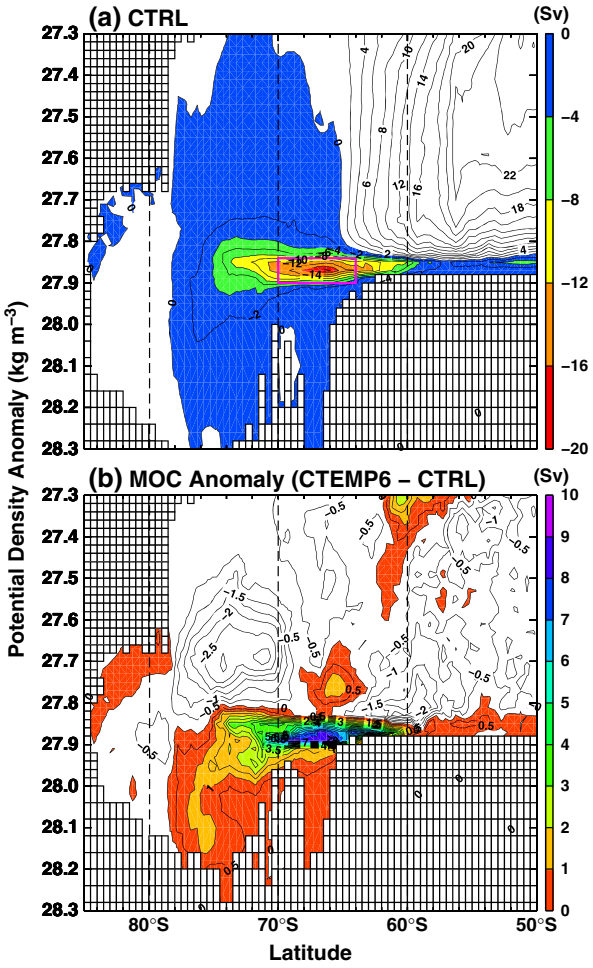


Figure 13. Stream function of zonally integrated, annual-mean meridional overturning circulation in the latitude-density domain. Positive contours indicate clockwise, negative contours anti-clockwise circulation. (a) The stream function in the CTRL case and (b) the anomaly of the stream function in the CTEMP6 case. The vertical axis indicates potential density anomaly referenced to the surface. In Figure 13a, positive and negative (with color shades) values indicate clockwise and anti-clockwise circulations. A pink box in Figure 13a indicates averaging area used in Figure 14. In Figure 13b, positive values are colored. Contour intervals of Figures 13a and 13b are 2.0 and 0.5 Sv, respectively.

and westerly winds over the Antarctic Circumpolar Current are modified (Table 1). In this model the basal melting is hardly affected by the change of westerly winds but depends sensitively on the surface air warming. Some recent studies suggested that the Antarctic Ice Sheet lose their mass [*Rignot et al.*, 2008, 2011; *Shepherd et al.*, 2012]. Importantly, ice shelf thinning or collapse could be triggered by enhanced basal melting as shown by this study and *Hellmer et al.* [2012], and such changes at marine termini of ice sheets can have large impacts on inland ice sheets [*Dupont and Alley*, 2005; *Schoof*, 2007; *Determann et al.*, 2012], leading to pronounced mass loss from the Antarctic Ice Sheet to the ocean.

[40] It should be mentioned that the basal melting could respond also to other atmospheric changes. A recent study of *Hellmer et al.* [2012] showed that basal melting of the Filchner-Ronne Ice Shelf would be enhanced drastically in this century by a combination of increases of air temperature and downward longwave radiation. We do not observe such a drastic increase of basal melting over the Filchner-Ronne Ice Shelf in our model even in the strongest warming case (CTEMP6). There is a possibility that the basal melting could respond more strongly or differently to future atmospheric changes in the real world.

[41] The magnitude of the response of basal melting to the surface air warming varies from region to region. The largest response is found at ice shelves in the Bellingshausen Sea, followed by those in the Eastern Weddell Sea and the Indian Sector (Figure 6). The reasons for enhanced basal melting of these ice shelves are increase of CDW and/or warm AASW into the ice shelf cavities (Figure 7). By contrast, the response of ice shelves in the Ross and Weddell Seas is insensitive to the warming. The reason for the insensitive basal melting is that active brine release accompanied with the high sea ice production at the front of the ice shelves can keep the water temperature to the surface freezing point even in the surface air warming experiments (Figure 7).

[42] In the model, the signal of the enhanced basal meltwater from the Amundsen and Bellingshausen Seas can be also traced to the bottom in the Australian Antarctic Basin (Figures 8 and 11). Active brine release at coastal polynyas in the Ross Sea (Figure 9) leads to active convection in winter and can convey the melt water signal to the bottom (Figure 8). In the real ocean, it has been reported that waters over the continental shelf in the Ross Sea and near bottom in the Australian-Antarctic Basin exhibit significant freshening

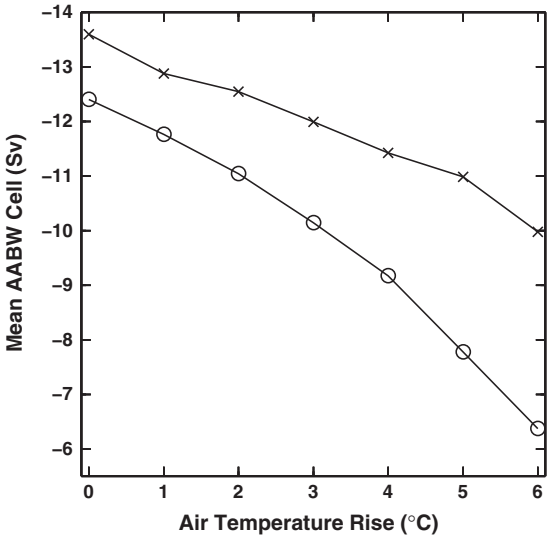


Figure 14. Response of the AABW cell to surface air warming (see Table 1 for the magnitude). Lines with circles and crosses indicate the experiments with and without the thermodynamic interaction under ice shelf, respectively. The magnitude of the AABW is calculated by averaging stream function over the density range of 27.84 to 27.90 kg m^{-3} and the latitude range of 64°S to 70°S (see the pink box in Figure 13a).

trends in the recent decades [*Aoki et al.*, 2005; *Rintoul*, 2007; *Shimada et al.*, 2012], and the causes for the freshening has been attributed to enhanced melting of the continental ices in the upstream regions [*Jacobs and Giulivi*, 2010]. From numerical experiments, we can clearly show that the enhanced melt water of the ice shelves in the Amundsen and Bellingshausen Seas can be a cause for freshening of waters in the Ross Sea and the Australian-Antarctic Basin, strongly supporting the previous observational findings.

[43] A similar mechanism, i.e., effect of upstream melt waters on downstream regions, may also happen in other sectors [*Thoma et al.*, 2010]. It is found that increased melt waters of ice shelves in the Eastern Weddell Sea play a role in freshening coastal waters over the continental shelf in the Weddell Sea and the signal spreads to the Scotia Sea (Figures 10 and 12).

[44] From a series of numerical experiments with and without the thermodynamic interaction under ice shelf, it is found that the enhanced melting of ice shelves strongly reduces the magnitude of the AABW cell (Figure 14). This result suggests that climate models without an ice shelf component tend to underestimate the response of the meridional overturning circulation related to AABW formation to future global warming.

[45] There are some limitations in our model. Ocean meso-scale eddies and tides would have an impact on ocean velocity fields under ice shelf. Since our model is a non-eddy resolving, non-tidal one, we use velocity-independent, constant thermal and salinity exchange velocities for solving the interaction between ice shelf and ocean. An eddy-resolving, tidal model with a velocity-dependent parameterization under ice shelf could yield different results. For example, although basal melting of ice shelves is not increased by enhanced westerly winds in our experiments, the response could be changed in an eddy-resolving, more sophisticated numerical model. Therefore, it would be an interesting, important, and challenging topic for future modeling research to investigate impacts of eddies and tides on ice shelf basal melting.

[46] The present model, whose horizontal resolution is about 10–20 km in Antarctic continental margins, can resolve all Antarctic ice shelves and produce the annual total melting amount and the basal melting/freezing pattern. This horizontal resolution can also reproduce high sea ice production in coastal regions (such as coastal polynyas), dense water mass formation there, and coastal currents, whereas coarse resolution models in previous studies do not reproduce these processes. The modeled basal melting of the Pine Island Glacier in this study (J5 in Figure A3) is much smaller than observational estimates (Table A4). It is considered that intrusions of warm water masses, such as Circumpolar Deep Water, guided by small scale topographies of a few kilometers play an important role in determining the high melt rate there. To resolve such small scale processes, the model with much higher resolution is required [*Heimbach and Losch*, 2012; *Schodlok et al.*, 2012].

Appendix A: Comparison of Modeled Basal Melting With Previous Studies

[47] Figures A1–A3 show a spatial distribution of basal melting/freezing of ice shelves in the ERA-INT case, which is an experiment driven by the surface forcings calculated from the ERA-Interim data set. Melting amount and mean melt rate for all ice shelves that are resolved in this model are listed in Table A1. In this Appendix, we compare our modeled basal melting for 10 major ice shelves with previous estimates (Tables A2–A4).

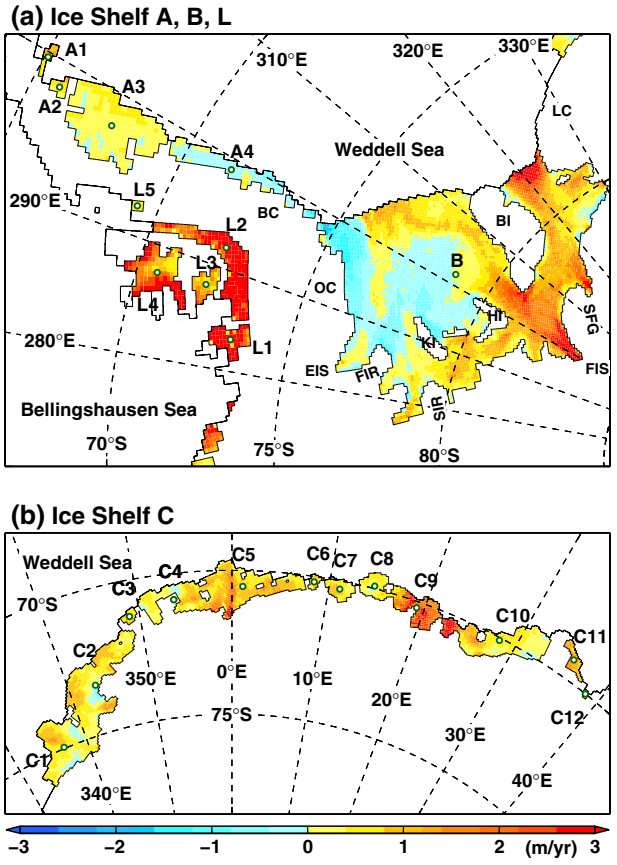


Figure A1. Spatial distribution of annual basal melting/freezing rate (m/yr) of ice shelves in the ERA-INT case in (a) the Bellingshausen and Weddell Seas and (b) Eastern Weddell Sea. Positive values indicate melting. Labels for ice shelf, such as A1, are listed in Table A1. Green circles indicate the center for each ice shelf. In Figure A1a, BC indicates Black Coast, OC Orville Coast, EIS Evans Ice Stream, FIR Fowler Ice Rise, SIR Skytrain Ice Rise, FIS Foundation Ice Stream, SFG Support Force Glacier, LC Luitpold Coast, KI Korff Ice Rise, HI Henry Ice Rise, and BI Berkner Island.

[48] We compare our basal melting amount also with an estimate of ice discharge, which corresponds to ice transport to the ocean across grounding lines. *Rignot et al.* [2008] estimated the ice discharge consistently almost all over the Antarctic Ice Sheet by using data of ice flow speed and ice thickness. Assuming a steady shape of ice shelf, no calving at the ice shelf edge, and negligible snow accumulation over the ice shelf, the amount of ice discharge coincides with that of basal melting at ice shelf. Of course, these assumptions are unrealistic. However, since there is no consistent estimate for basal melting over Antarctic ice shelves at this point of time, we use the ice discharge calculated by *Rignot et al.* [2008] as a measure of an upper limit of basal melting amount [see *Rignot et al*. 2008, supplementary material].

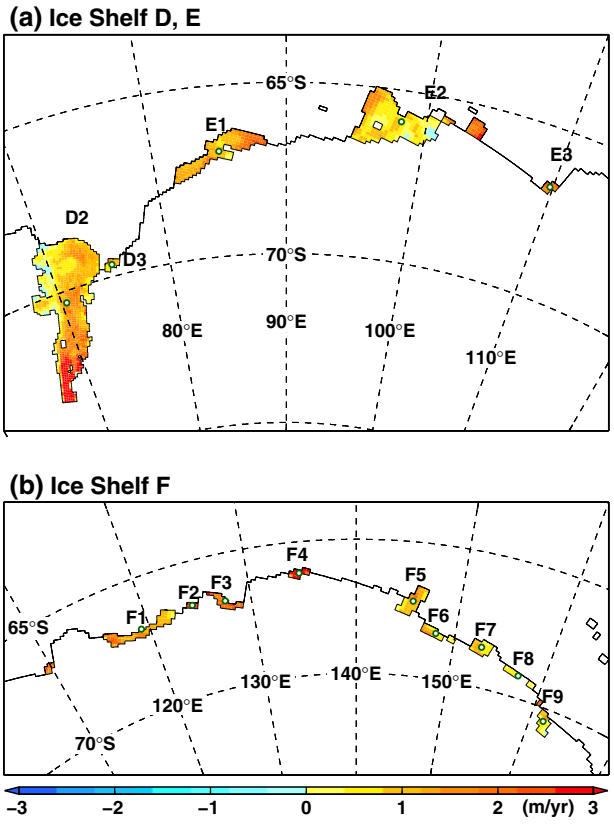


Figure A2. Same as Figure A1, but for ice shelves in East Antarctica.

A1. Larsen C Ice Shelf (A3)

[49] The Larsen Ice Shelves are fringing ice shelves on the eastern side of the Antarctic Peninsula. The Larsen C Ice Shelf is the largest one among them. Our model estimates for this ice shelf are 10–12 Gt/yr for the basal melting amount and 0.2 m/yr for the mean melt rate. Previous estimates range widely between 6 and 70 Gt/yr for the melting amount (model ensemble mean: 34 Gt/yr) and between 0.1 and 1.3 m/yr for the mean melt rate (Table A2). The ice discharge of *Rignot et al.* [2008] into this ice shelf is 45.5 Gt/yr. Our basal melting amount is lower than the ice discharge estimate, indicating that our estimate for the Larsen C Ice Shelf is possible.

[50] It should be noted that there is a predominant freezing area along the Black Coast (A4 in Figure A1). This freezing area is formed by a direct inflow of ISW exported from the Ronne Ice Shelf (Figure 5).

A2. Filchner-Ronne Ice Shelf (B)

[51] The Filchner-Ronne Ice Shelf is the second largest ice shelf in Antarctica in terms of areal extent. We estimate 161–191 Gt/yr for the total melting amount and 0.4–0.5 m/yr for the mean melt rate over the Filchner-Ronne Ice Shelf. Estimates of previous observational and modeling studies are 40–202 Gt/yr (mean: 116 Gt/yr) and 40–438 Gt/yr (mean: 132 Gt/yr), respectively (Table A2). Our estimate is larger than the ensemble means of previous observational and modeling estimates. The ice discharge of *Rignot et al.* [2008] into the Filchner-Ronne Ice Shelf is 221 Gt/yr. Our basal melting amount is lower than the ice discharge estimate.

[52] *Joughin and Padman* [2003] estimated a spatial distribution of basal melting/freezing over the most part of the Filchner-Ronne Ice Shelf from remote-sensing data set with an assumption of steady shape of the ice shelf [see *Joughin and Padman* 2003, Figure 2]. Our model roughly reproduces the basal melting/freezing pattern in the following three points. First, there are an extensive freezing area north of the Henry and Korff Ice Rises and a freezing area between the southern part of the Oriville Coast and the Fowler Ice Rise. Second, melting areas are reproduced in the eastern, southeastern, and southern sides of the ice shelf near the grounding line. Third, an active melting area is found along the ice front northwest of the Berkner Island. However, there is one notable difference between the model and the observed spatial pattern. In the northwestern part of the Ronne Ice Shelf (area off the northern part of the Orville Coast), the model shows strong freezing, but the observation shows melting.

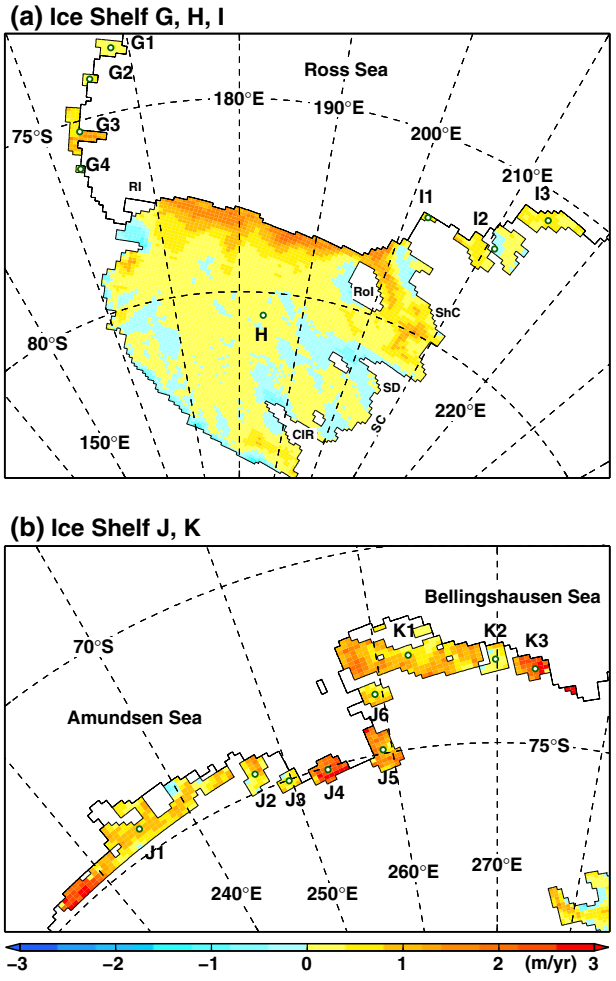


Figure A3. Same as Figure A1, but for ice shelves in (a) the Ross Sea and (b) the Bellingshausen Sea. In Figure A3a, RI indicates Ross Island, RoI Roosevelt Island, CIR Crary Ice Rise, SC Siple Coast, SD Siple Dome, and ShC Shirase Coast.

Table A1. Details of Basal Melting Amount and Mean Melt Rate for Antarctic Ice Shelves[a]

Region		Name or Place name	AREA ($\times 10^3$km^2)	Longitude (°E)	Latitude (°S)	Melting Amount[b] (Gt/yr)	Mean Melt Rate[c] (ice, m/yr)
A	A1	Larsen A	2.7	299.65	65.09	9.7(2.3)	3.99(0.94)
	A2	Larsen B	2.8	298.19	65.81	2.4(1.5)	0.91(0.57)
	A3	Larsen C	56.5	297.45	67.69	10.2(12.0)	0.20(0.23)
	A4	(Black Coast)	23.6	298.98	71.43	–0.7(–3.1)	–0.03(–0.14)
B	B	Filchner-Ronne	438.1	301.64	78.85	160.5(190.7)	0.40(0.47)
C	C1	Brunt	32.7	336.76	74.95	3.9(13.8)	0.13(0.46)
	C2	Riiser-Larsen	48.7	343.22	73.29	13.9(23.9)	0.31(0.53)
	C3	Quarisen	2.4	348.89	71.25	1.0(1.7)	0.46(0.76)
	C4	Ekstrom-Jelbart	21.4	353.83	70.91	4.7(10.2)	0.24(0.52)
	C5	Fimbulisen	40.6	1.15	70.55	20.3(37.7)	0.54(1.01)
	C6	Vigridsen	2.0	8.43	70.19	1.3(1.6)	0.69(0.88)
	C7	Nivlisen	7.2	11.13	70.28	3.6(4.4)	0.55(0.66)
	C8	17E Glacier	8.9	14.52	69.91	1.8(3.2)	0.22(0.39)
	C9	Borchgrevinkisen	17.0	19.20	70.21	26.5(29.0)	1.70(1.86)
	C10	26E Glacier	36.5	28.25	70.09	25.6(23.6)	0.76(0.70)
	C11	(Prince Harald Coast)	5.0	35.58	69.30	3.6(5.6)	0.79(1.21)
	C12	Shirase Glacier	0.6	38.53	70.00	0.4(0.6)	0.69(1.00)
	C13	(Casey Bay)	0.7	48.29	67.34	1.0(1.1)	1.59(1.70)
D	D1	Seaton-Robert Glaciers	1.5	56.54	66.95	2.9(2.1)	2.20(1.61)
	D2	Amery	65.2	70.42	70.33	67.0(79.8)	1.12(1.34)
	D3	Polar Times Glacier	1.4	75.10	69.65	0.4(1.1)	0.27(0.87)
E	E1	West	16.1	84.99	66.92	12.3(19.4)	0.83(1.31)
	E2	Shackleton	32.5	98.21	65.91	12.7(24.6)	0.43(0.82)
	E3	(Vincennes Bay)	1.4	109.77	66.71	2.1(2.3)	1.64(1.82)
F	F1	Moscow University	11.2	119.21	66.88	10.8(13.3)	1.05(1.30)
	F2	(Paulding Bay)	1.1	124.46	66.63	2.0(2.3)	1.97(2.30)
	F3	Holmes Glacier	4.3	127.56	66.79	4.5(8.1)	1.14(2.04)
	F4	Dibble Glacier	2.6	134.72	66.16	6.6(6.8)	2.81(2.90)
	F5	Mertz Glacier	8.0	145.45	67.20	10.7(7.8)	1.46(1.07)
	F6	Ninnis Glacier	4.2	148.05	68.29	2.2(2.9)	0.56(0.76)
	F7	Cook	4.8	152.86	68.50	3.0(3.6)	0.69(0.81)
	F8	(Wilson Hills)	2.6	157.28	69.17	0.7(0.9)	0.30(0.37)
	F9	Rennick Glacier	4.6	161.49	70.47	3.0(3.1)	0.71(0.72)
G	G1	Mariner Glacier	3.2	168.41	73.37	2.2(0.7)	0.73(0.23)
	G2	(lady Newnes Bay)	1.1	165.89	74.03	0.9(0.3)	0.86(0.31)
	G3	Drygalski Ice Tongue	6.5	163.63	75.27	9.4(5.3)	1.57(0.89)
	G4	(Scott Coast)	0.5	162.56	76.20	0.4(0.3)	0.96(0.73)
H	H	Ross	479.8	183.78	80.59	110.7(94.1)	0.25(0.21)
I	I1	(Edward VII Peninnsula)	0.6	202.43	77.11	0.2(0.3)	0.42(0.55)
	I2	Sulzberger Ice Shelf	14.5	210.94	77.06	2.5(3.3)	0.18(0.25)
	I3	(Rupert Coast)	8.2	214.23	75.70	2.2(3.3)	0.29(0.44)
J	J1	Getz	36.5	235.26	74.37	34.6(30.3)	1.03(0.91)
	J2	Dotson	5.4	247.00	74.56	4.5(3.1)	0.90(0.62)
	J3	Smith Glacier	2.7	249.75	75.02	0.9(1.3)	0.36(0.52)
	J4	Thwaites Glacier Tongue	5.4	253.59	75.06	8.2(10.4)	1.65(2.09)
	J5	Pine Island Glacier	7.8	259.14	74.91	8.2(10.2)	1.15(1.43)
	J6	Cosgrove	4.1	259.36	73.53	2.4(2.8)	0.66(0.75)
K	K1	Abbot	32.8	262.62	72.71	60.5(29.8)	2.01(0.99)
	K2	(Fletcher Peninsula)	4.2	269.84	72.95	3.2(1.1)	0.84(0.29)
	K3	Venable	5.3	273.22	73.16	4.8(10.2)	0.98(2.08)
L	L1	Stange	10.5	283.29	73.25	9.9(35.6)	1.02(3.69)
	L2	George VI	29.5	292.00	72.30	45.1(104.6)	1.66(3.86)
	L3	Bach	7.2	287.97	72.10	1.6(7.6)	0.24(1.15)
	L4	Wilkins	22.7	287.65	70.61	25.8(50.7)	1.24(2.43)
	L5	Wordie	1.3	292.47	69.38	1.0(0.6)	0.83(0.54)
		Total	1598.6	-	-	769.6(943.8)	0.52(0.64)

[a]The non-parenthesized (parenthesized) values indicate the CTRL (ERA-INT) case. See green circles in Figures A1–A3 for locations of ice shelves. Place names are in the parentheses.

[b]An ocean reference density is 1028 kg m^{-3}.

[c]The value is a melt rate for the ice shelf base. An ice shelf reference density is 917 kg m^{-3}.

Table A2. Comparison of Ice Shelf Basal Melting With Previous Studies for the Larsen C, Filchner-Ronne, Brunt-Riiser-Larsen, Jelbart-Fimbulisen Ice Shelves[a]

Ice Shelf	Amount	Rate	Method
Larsen C (A3)	**(Gt/yr)**	**(m/yr)**	
This study	10–12	0.20–0.23	CM
Timmermann et al. [2012]	48	1.0	CM
Mueller et al. [2012]	6–24	0.11–0.44	RM
Holland et al. [2009]	15–70	0.27–1.26	RM
Hellmer [2004]	38	0.63	CM (including Larsen B)
Filchner-Ronne (B)	**(Gt/yr)**	**(m/yr)**	
This study	161–191	0.40–0.47	CM
Timmermann et al. [2012]	138	0.35	CM
Hellmer et al. [2012]	82	0.2	CM
Makinson et al. [2011]	92	0.22	RM
Olbers and Hellmer [2010]	–	0.6–1.2	Box model (Filchener)
Olbers and Hellmer [2010]	–	0.2–0.5	Box model (Ronne)
Nicholls et al. [2009]	*81–137*[b,c]	0.20–0.34	O
Losch [2008]	438	0.94	CM
Hellmer [2004]	120	0.32	CM
Nicholls et al. [2003]	158	0.34±0.1	O
Joughin and Padman [2003]	83 ± 25	0.19 ± 0.06	S
Foldvik et al. [2001]	100	0.2	O
Gerdes et al. [1999]	40–50	0.10	RM
Grosfeld and Gerdes [1998]	92	0.21	RM
Gammelsrød et al. [1994]	*40*[b,c]	0.1	O
Jacobs et al. [1992]	202	0.55[d]	G
Schlosser et al. [1990]	126	0.3	O
Brunt and Riiser-Larsen (C1+C2)	**(Gt/yr)**	**(m/yr)**	
This study	18–38	0.24–0.50	CM
Timmermann et al. [2012]	65	0.94	RM
Thoma et al. [2006]	66	0.88	CM
Hellmer [2004]	166	2.38	CM
Fahrbach et al. [1994]	–	< 2.3	O
Jelbart and Fimbulisen (C4+C5)	**(Gt/yr)**	**(m/yr)**	
This study	25–48	0.44–0.84	CM
Timmermann et al. [2012]	130	2.80	CM
Humbert [2010]	–	< 0.6 (most parts)	RM
Olbers and Hellmer [2010]	–	0.5–1.2	Box model (Fimbulisen)
Nicholls et al. [2008]	–	0.85	RM (Fimbulisen)
Smedsrud et al. [2006]	139	1.9	RM
Hellmer [2004]	243	4.91	CM

[a]In the 'Method' column, CM stands for a circumpolar model, RM a regional model, G glaciological estimate, O oceanographic estimate, S satellite estimate. Italic values are converted from the basal melting amount or rate in the literature with some assumptions.

[b]An ice density of 917 kg m^{-3} is assumed.

[c]440×10^3 km^2 is assumed.

[d]The mean melt rate is derived from *Jenkins and Doake* [1991]

[53] It should be noted that our basal melting/freezing pattern over the Filchner-Ronne Ice Shelf agrees well with that of a recent high resolution model study by *Timmermann et al.* [2012]. Their model also showed that basal freezing dominates over the northwestern part of the Ronne Ice Shelf. In our model there is an export of ISW from the northern part of the Ronne Ice Shelf. The existence of freezing area is physically consistent with the ISW export. An observation of *Nicholls et al.* [2004] suggested northward export of ISW from the Ronne Ice Shelf.

A3. Eastern Weddell Ice Shelves (C)

[54] The Eastern Weddell Ice Shelves are composed of many small ice shelves in a longitude range from 30°W (330°E) to 40°E. The Brunt and Riiser-Larsen Ice Shelves (C1 and C2) located in the western side are the largest ones in the Eastern Weddell Ice Shelves. We estimate 18–38 Gt/yr for the total melting amount and 0.2–0.5 m/yr for the mean melt rate. Previous modeling studies estimated 65–166 Gt/yr (mean: 99 Gt/yr) for the basal melting amount (Table A2) and all of these estimates are higher than our estimates. The ice discharge estimate of *Rignot et al.* [2008] into the Brunt and Riiser-Larsen Ice Shelves is 44 Gt/yr, supporting that our estimate is possible.

[55] The Jelbart and Fimbulisen Ice Shelves (C4 and C5) cross the Prime Meridian and are the second largest ones in the Eastern Weddell Ice Shelves in terms of areal extent. We estimate 25–48 Gt/yr for the total melting amount and 0.4–0.8 m/yr for the mean melt rate. As in the case of the Riiser-Larsen Ice Shelves, our estimate of basal melting for the Jelbart and Fimbulisen Ice Shelves is lower than those of previous modeling studies (range: 130–243 Gt/yr, mean: 171 Gt/yr). The ice discharge estimate of *Rignot et al.* [2008] into these ice shelves is 28 Gt/yr. Our basal

Table A3. Same as Table A2, but for the Amery and Ross Ice Shelves

Ice Shelf	Amount	Rate	Method
Amery (D2)	**(Gt/yr)**	**(m/yr)**	
This study	67–80	1.12–1.34	CM
Timmermann et al. [2012]	174	2.9	CM
Galton-Fenzi et al. [2012]	46	0.74	RM
Olbers and Hellmer [2010]	–	1.1–2.2	Box model
Wen et al. [2010]	46±7	*0.84*[a,b]	S
Yu et al. [2010]	27±7	*0.49*[a,b]	S
Hellmer [2004]	18	0.35	CM
Williams et al. [2001]	6–18	0.11–0.35	RM
Hellmer and Jacobs [1992]	23	0.65	RM
Ross (H)	**(Gt/yr)**	**(m/yr)**	
This study	94–111	0.21–0.25	CM
Timmermann et al. [2012]	260	0.6	CM
Dinniman et al. [2011]	*67*[a,b]	0.15	RM
Olbers and Hellmer [2010]	–	0.2	Box model
Reddy et al. [2010]	*44*[a,b]	0.10	RM
Loose et al. [2009]	33–50	*0.07-0.11*[a,b]	O
Dinniman et al. [2007]	*59*[a,b]	0.13	RM
Smethie and Jacobs [2005]	60[c]	*0.18*[a,b,c]	O
Hellmer [2004]	180	0.49	CM
Assmann et al. [2003]	167	0.41	RM
Holland et al. [2003]	*36*[a,b]	0.08	RM
Jacobs et al. [1992]	79	0.22	O, RM
Lingle et al. [1991]	*75*[a,b]	0.17	RM
Shabtaie and Bentley [1987]	60±15	0.12±0.03	Radar
Pillsbury and Jacobs [1985]	150	*0.34*[a,b]	O

[a]An ice density of 917 kg m^{-3} is assumed.
[b]Areas of 60 × 10^3 km^2 for the Amery Ice Shelf and 480 × 10^3 km^2 for the Ross Ice Shelf are assumed.
[c]Area of the Ross Ice Shelf exceeding the 300-m draft (75%).

melting estimates are comparable to or slightly larger than the ice discharge. *Nicholls et al.* [2008] suggested a possibility of overestimate of their modeled mean basal melt rate at 0.85 m/yr for the Fimbulisen Ice Shelf from comparison of observational and modeled ocean properties. Moreover, *Humbert* [2010] estimated the melt rate lower than 0.6 m/yr over most parts of the Fimbulisen Ice Shelf from horizontal divergence of ice volume flux and surface accumulation under an assumption of the steady shape of ice shelf. Therefore, our estimates for these ice shelves are possible.

[56] Note that the highest basal melt rate in the Eastern Weddell Ice Shelves is found in the ice shelf C9 with a value of 1.7–1.9 m/yr. Our two experiments show commonly this feature. The areas coincide with the thinning ice shelves recently reported by *Pritchard et al.* [2012].

A4. Amery Ice Shelf (D)

[57] The modeled total basal melting over the Amery Ice Shelf is 67–80 Gt/yr, which is larger than the observational estimates, 27–46 Gt/yr (mean: 37 Gt/yr) [*Wen et al.*, 2010; *Yu et al.*, 2010]. The previous modeling estimates are in a wide range from 6 to 174 Gt/yr (mean: 48 Gt/yr). The ice discharge estimate of *Rignot et al.* [2008] into the Amery Ice Shelves is 78 Gt/yr. Thinning of ice shelf is observed on the eastern side of the Amery Ice Shelf [*Pritchard et al.*, 2012]. Assuming the rate of ice shelf thinning at 1.0 m/yr over about one-third of the area of the Amery Ice Shelf ($22 \times 10^3 km^2$), an ice amount of 20 Gt/yr should be added to the above ice discharge, so the total ice sheet-origin ice to melt in the ocean would be about 98 Gt/yr. Our estimate of the basal melting over the Amery Ice Shelf is under the upper limit.

[58] *Wen et al.* [2010] estimated the spatial distribution of basal melting/freezing over the Amery Ice Shelf from remote-sensing data set with an assumption of steady shape of the ice shelf. The observational pattern shows a freezing area in the northwestern parts and a high melting area in the eastern and southern parts [see *Wen et al* 2010, Figure 6]. Our model roughly shows this pattern, but the modeled freezing area is much smaller than the observational one. There is a possibility that lack of frazil ice formation process in this model leads underestimation of basal freezing. A recent study of the Amery Ice Shelf investigated impact of frazil ice formation on basal melting and showed that the net melting over the ice shelf is reduced by about 10% when compared with a simulation without frazil ice formation [*Galton-Fenzi et al.*, 2012]. Therefore, the modeled net basal melting is overestimated when compared with observational estimates.

Table A4. Same as Table A2, but for the Getz, Abbot Ice Shelves, the Pine Island Glacier, and the George VI Ice Shelf

Ice Shelf	Amount	Rate	Method
Getz (J1)	**(Gt/yr)**	**(m/yr)**	
This study	30–35	0.91–1.03	CM
Timmermann et al. [2012]	164	5.4	CM
Schodlok et al. [2012]	171	23.03	RM
Olbers and Hellmer [2010]	–	14–15	Box model
Hellmer [2004]	54	1.95	CM
Pine Island Glacier (J5)	**(Gt/yr)**	**(m/yr)**	
This study	8–10	1.15–1.43	CM
Timmermann et al. [2012]	13	3.1	CM
Schodlok et al. [2012]	118	28.28	RM
Heimbach and Losch [2012]	–	21.89	RM
Jacobs et al. [2011]	53–85	22–33	O
Olbers and Hellmer [2010]	–	23–30	Box model
Shepherd et al. [2004]	–	15±2	S
Rignot [1998]	–	24±4	S
Jenkins et al. [1997]	28	12±3	G, O
Jacobs et al. [1996]	28	10–12	O
Abbot (K1)	**(Gt/yr)**	**(m/yr)**	
This study	30–61	0.99–2.01	CM
Timmermann et al. [2012]	59	2.1	CM
Schodlok et al. [2012]	62	5.59	RM
Holland et al. [2010]	*31*[a,b]	1.01	RM
Hellmer [2004]	18	0.55	CM
George VI (L2)	**(Gt/yr)**	**(m/yr)**	
This study	44–105	1.6–3.86	CM
Timmermann et al. [2012]	86	3.6	CM
Dinniman et al. [2012]	*133*[a,b]	5.8	RM
Dinniman et al. [2011]	*138*[a,b]	6.0	RM
Holland et al. [2010]	*57*[a,b]	2.49	RM
Jenkins and Jacobs [2008]	78–119	3.1–4.8	O
Hellmer [2004]	22	0.43	CM
Corr et al. [2002]	*64*[ab]	2.78±0.08	G, Radar
Potter et al. [1984]	53	2	G, O

[a]An ice density of 917 kg m^{-3} is assumed.
[b]Areas of 33 × 10^5 km^2 for the Abbot Ice Shelf and 25 × 10^3 km^2 for the George VI Ice Shelf are assumed.

A5. Ice Shelves in Longitude From 80°E to 165°E (E and F)

[59] There are small ice shelves separately in longitudes from 80°E to 165°E. We estimate 27–46 Gt/yr and 44–49 Gt/yr for the basal melting amount over ice shelves of E and F, respectively. Until now, there is no study that focuses on basal melting of these ice shelves and no consensus exists for basal melting there. The ice discharge estimates of *Rignot et al.* [2008] into the ice shelves of E and F are 87 and 301 Gt/yr, respectively. Since our basal melting amounts over these ice shelves are lower than the ice discharges, our estimates are possible values.

A6. The Ross Sea (H)

[60] We estimate 94–111 Gt/yr for the total melting amount over the Ross Ice Shelf. The previous estimates of observational and modeling studies are 33–150 Gt/yr (mean: 74 Gt/yr) and 36–260 Gt/yr (mean: 111 Gt/yr), respectively (Table A3). The ice discharge estimate of *Rignot et al.* [2008] into the Ross Ice Shelf is 129 Gt/yr. There is no significant change of ice shelf thickness [*Pritchard et al.*, 2012], therefore the ice discharge can be considered to be a upper limit of basal melting. Since our estimate is lower than the upper limit, our estimates are possible.

[61] The modeled melting rate increases exponentially northward to the ice front (Figure A3a). The modeled melting pattern is consistent with the observational results of *Horgan et al.* [2011] who estimated basal melting rates near the ice front from altimeter data set. There are inactive areas in the central parts of the Ross Ice Shelf. A net freezing area is found in the area west of the Siple Dome and area along the southeastern coastline. This distribution is consistent with a melting/freezing pattern suggested by *Zotikov et al.* [1980]. There is a basal melting area south of the Crary Ice Rise. The melting/freezing spatial pattern in this model is generally consistent with previous modeling studies [*Holland et al.*, 2003; *Dinniman et al.*, 2007; *Reddy et al.*, 2010].

A7. The Amundsen Sea (J)

[62] The Getz Ice Shelf (J1) is the largest ice shelf in the Amundsen Sea. We estimate 30–35 Gt/yr for the total melting amount and 0.9–1.0 m/yr for the mean melt rate. Our model underestimates the basal melting there, as explained below. *Rignot et al.* [2008] estimated 98 Gt/yr for the ice discharge into the ice shelf. *Pritchard et al.* [2012] reported that the thickness over the Getz Ice Shelf is thinning at a rate of more than 3 m/yr. Therefore, basal melting should be larger than the ice discharge at least to explain the thinning trend. A recent modeling study of *Timmermann et al.* [2012] showed a high basal melting amount over the Getz Ice Shelf (164 Gt/yr). Their result is consistent with the recent thinning trend of ice shelf thickness.

[63] The Pine Island Glacier (J5) is known as an ice shelf showing the highest melt rate around the Antarctic ice shelves. We estimate 8–10 Gt/yr for the total melting amount over the Pine Island Glacier and 1.2–1.4 m/yr for the mean melt rate. Our modeled values are much smaller than those estimated from observations (range: 28–85 Gt/yr, mean: 49 Gt/yr) and recent high resolution regional models (range: 13–118 Gt/yr, mean: 66 Gt/yr) [*Heimbach and Losch*, 2012; *Schodlok et al.*, 2012].

[64] Our model tends to underestimate the basal melting of ice shelves in the Amundsen Sea. We consider that a cause of this bias is insufficient horizontal resolution. The high basal melt rate at ice shelves in the Amundsen Sea is considered to be achieved by intrusions of warm CDW across the shelf breaks. The horizontal resolution in our model for this area is about 20 km, therefore the model can not sufficiently resolve key topography that guides the CDW into inner continental shelf.

A8. Abbot Ice Shelf (K1)

[65] The Abbot Ice Shelf is the largest ice shelf in the Bellingshausen Sea. We estimate 30–61 Gt/yr for the total melting amount and 1.0–2.0 m/yr for the mean melt rate, being consistent with previous modeling estimates of 18–62 Gt/yr (mean: 43 Gt/yr). *Rignot et al.* [2008] estimated 32 Gt/yr for the ice discharge into the ice shelf. Since there is no significant change of the ice shelf thickness over the ice shelf [*Pritchard et al.*, 2012], and the ice discharge is considered to be the upper limit of basal melting. Our estimate of basal melting for the Abbot Ice Shelf in the ERA-INT case is possible, but that in CTRL case seems to be slightly overestimated.

A9. George VI Ice Shelf (L2)

[66] The George VI Ice Shelf is bounded to the west and the east by the Alexander Island and the Antarctic Peninsula. We estimate 44–105 Gt/yr for the total melting amount over the George VI Ice Shelf and 1.7–3.9 m/yr for the mean melt rate. The basal melting at the George VI Ice Shelf in the ERA-INT case is larger than that in the CTRL case. This is explained by differences of the water masses into the cavity. In the CTRL case, MSW is a dominant water mass into the ice shelves of L. In the ERA-INT case, on the other hand, MCDW dominates the inflow, leading to the larger basal melting.

[67] Previous estimates of observations and modeling study are 53–119 Gt/yr (mean: 79 Gt/yr) and 22–138 Gt/yr (mean: 87 Gt/yr), respectively (Table A4). Our estimate is in a range of the previous estimates. *Rignot et al.* [2008] estimated 78 Gt/yr for the ice discharge into the ice shelf. *Pritchard et al.* [2012] reported that the thickness of the George VI Ice Shelf over the southern part is thinning [*Pritchard et al.*, 2012]. Assuming thinning of ice shelf thickness at 1.5 m/yr over about two-thirds of the area of the George VI Ice Shelf (17×10^3 km^2), an ice amount of 23 Gt/yr should be added the above ice discharge and the total ice to melt in the ocean would be about 101 Gt/yr. Therefore, our estimate of basal melting for the George VI Ice Shelf is considered to be a possible one. It should be noted that the area of the George VI Ice Shelf in our model (29.5×10^3 km^2) is slightly larger than that in the real ice area shelf [25×10^3 km^2, *Potter and Paren*, 1985], because the coastline in the model is modified to resolve the narrow sound in the northern part.

[68] **Acknowledgments.** Numerical calculations were performed on FX10 and HA8000 at Information Technology Center, the University of Tokyo. We thank two anonymous reviewers for their careful reading and constructive comments on the manuscript. This study is supported by JST/CREST, JSPS/KAKENHI, and the Sasagawa Scientific Research Grant from The Japan Science Society.

References

Adcroft, A., C. Hill, and J. Marshall (1997), Representation of topography by shaved cells in a height coordinate ocean model, *Mon. Weather Rev.*, *125*(9), 2293–2315.

Aoki, S., S. R. Rintoul, S. Ushio, S. Watanabe, and N. L. Bindoff (2005), Freshening of the Adélie Land Bottom Water near 140°E, *Geophys. Res. Lett.*, *32*, L23,601, doi:10.1029/2005GL024246.

Assmann, K., H. H. Hellmer, and A. Beckmann (2003), Seasonal variation in circulation and water mass distribution on the Ross Sea continental shelf, *Antarct. Sci.*, *15*(1), 3–11, doi:10.1017/S0954102003001007.

Assmann, K. M., and R. Timmermann (2005), Variability of dense water formation in the Ross Sea, *Ocean Dynam.*, *55*, 68–87, doi:10.1007/s10236-004-0106-7.

Beckmann, A., H. H. Hellmer, and R. Timmermann (1999), A numerical model of the Weddell Sea: Large-scale circulation and water mass distribution, *J. Geophys. Res.*, *104*(C10), 23,375–23,391.

Boyer, T. P., S. Levitus, J. I. Antonov, R. A. Locarnini, and H. E. Garcia (2005), Linear trends in salinity for the world ocean, 1955–1998, *Geophys. Res. Lett.*, *32*, L01,604, doi:10.1029/2004GL021791.

Bracegirdle, T. J., W. M. Connolley, and J. Turner (2008), Antarctic climate change over the twenty first century, *J. Geophys. Res.*, *114*, D03,103, doi:10.1029/2007JD008933.

Corr, H. F. J., A. Jenkins, K. W. Nicholls, and C. S. M. Doake (2002), Precise measurement of changes in ice-shelf thickness by phase-sensitive radar to determine basal melt rates, *Geophys. Res. Lett.*, *29*(8), 1232, doi:10.1029/2001GL014618.

Dee, D. P., et al. (2011), The ERA-Interim reanalysis: Configuration and performance of the data assimilation system, *Q. J. Roy. Meteor. Soc.*, *137*(656), 553–597, doi:10.1002/qj.828.

Determann, J., M. Thoma, K. Grosfeld, and S. Massmann (2012), Impact of ice-shelf basal melting on inland ice-sheet thickness: A model study, *Ann. Glaciol.*, *53*(60), 129–135, doi:10.3189/2012AoG60A170.

Dinniman, M. S., J. M. Klinck, and W. O. Smith Jr. (2007), Influence of sea ice cover and icebergs on circulation and water mass formation in a numerical circulation model of the Ross Sea, Antarctica, *J. Geophys. Res.*, *112*, C11,013, doi:10.1029/2006JC004036.

Dinniman, M. S., J. M. Klinck, and W. O. Smith Jr. (2011), A model study of circumpolar deep water on the West Antarctic Peninsula and Ross Sea continental shelves, *Deep-Sea Res. Pt. II*, *58*, 1508–1523, doi:10.1016/j.dsr2.2010.11.013.

Dinniman, M. S., J. M. Klinck, and E. E. Hofmann (2012), Senitivity of Circumpolar Deep Water transport and ice shelf basal melt along the West Antarctic Peninsula to changes in the winds, *J. Climate*, *25*, 4799–4816, doi:10.1175/JCLI-D-11-00307.1.

Drewry, D. J., S. R. Jordan, and E. Jankowski (1982), Measured properties of the Antarctic Ice Sheet: Surface configuration, ice thickness, volume and bedrock characteristics, *Ann. Glaciol.*, *3*, 83–91.

Drucker, R., S. Martin, and R. Kwok (2011), Sea ice production and export from coastal polynyas in the Weddell and Ross Seas, *Geophys. Res. Lett.*, *38*, L17,502, doi:10.1029/2011GL048668.

Dupont, T. K., and R. B. Alley (2005), Assessment of the importance of ice-shelf buttressing to ice-sheet flow, *Geophys. Res. Lett.*, *32*, L04,503, doi:10.1029/2004GL022024.

Fahrbach, E., R. G. Peterson, G. Rohardt, P. Schlosser, and R. Bayer (1994), Suppression of bottom water formation in the southeastern Weddell Sea, *Deep-Sea Res. Pt. II*, *41*(2), 389–411.

Foldvik, A., T. Gammelsrød, E. Nygaard, and S. Østerhus (2001), Current measurments near Ronne Ice Shelf: implications for circulation and melting, *J. Geophys. Res.*, *106*, 4463–3377.

Fox, A. J., and A. P. R. Cooper (1994), Measured properties of the Antarctic ice sheet derived from the SCAR Antarctic digital database, *Polar Rec.*, *39*, 201–206, doi:10.1017/S0032247400024268.

Fyfe, J. C., and O. A. Saenko (2006), Simulated changes in the extratropical Southern Hemisphere winds and currents, *Geophys. Res. Lett*, *33*, L06,701, doi:10.1029/2005GL025332.

Gade, H. G. (1979), Melting of ice in sea water: A primitive model with application to the Antarctic ice shelf and icebergs, *J. Phys. Oceanogr.*, *9*, 189–198.

Galton-Fenzi, B. K. (2010), Modelling interactions between Antarctica and the Southern Ocean, *Aust. Antarct. Mag.*, *19*, 6 pp.

Galton-Fenzi, B. K., J. R. Hunter, R. Coleman, S. J. Marsland, and R. C. Warmer (2012), Modeling the basal melting and marine ice accretion of the Amery Ice Shelf, *J. Geophys. Res.*, *117*, C09,031, doi:10.1029/2012JC008214.

Gammelsrød, T., A. Foldvik, O. A. Nøst, Ø. Skagset, L. G. Anderson, E. Fogelqvist, T. Tanhua, E. P. Jones, and S. Østerhus (1994), Distribution of water masses on the continental shelf in the southern Weddell Sea, in *The Polar Oceans and their Role in Shaping the Global Environment*, 159–176 pp., AGU, Washington, D.C.

Gent, P. R., J. Willbrand, T. J. McDougall, and J. C. McWilliams (1995), Parameterizing eddy-induced tracer transports in ocean circulation models, *J. Phys. Oceanogr.*, *25*, 463–474.

Gerdes, R., J. Determann, and K. Grosfeld (1999), Ocean circulation beneath Filchner-Ronne Ice Shelf from three-dimensional model results, *J. Geophys. Res.*, *104*, 15,827–15,842.

Gille, S. T. (2002), Warming of the Southern Ocean since the 1950s, *Science*, *295*, 1275–1277.

Grosfeld, K., and R. Gerdes (1998), Circulation in the Filchner-Ronne Ice Shelf domain: First results from a 3D-ocean model, *Filchner-Ronne Ice Shelf Programme*, *12*, 35–39.

Hasumi, H., (2006), CCSR Ocean Component Model (COCO) version 4.0, *CCSR Report 25*, Center for Climate System Research, University of Tokyo.

Hattermann, T., O. A. Nøst, J. M. Lilly, and L. H. Smedsrud (2012), Two years of oceanic observations below the Fimbul Ice Shelf, Antarctica, *Geophys. Res. Lett.*, *39*, L12,605, doi:10.1029/2012GL051012.

Heimbach, P., and M. Losch (2012), Adjoint sensitivities of sub-ice-shelf melt rates to ocean circulation under the Pine Island Ice Shelf, West Antarctica, *Ann. Glaciol.*, *53* (60), 59–69, doi:10.3189/2012/AoG60A025.

Hellmer, H. H. (2004), Impact of Antarctic ice shelf basal melting on sea ice and deep ocean properties, *Geophys. Res. Lett.*, *31*, L10,307, doi:10.1029/2004GL019506.

Hellmer, H. H., and S. S. Jacobs (1992), Ocean interactions with the base of Amery Ice Shelf, Antarctica, *J. Geophys. Res.*, *97*, 20,305–20,317.

Hellmer, H. H., and S. S. Jacobs (1994), Temporal changes in shelf water of the southern Ross Sea, *Antarc. J. of the U.S.*, *29*(5), 123–124.

Hellmer, H. H., and D. J. Olbers (1989), A two-dimensional model for the thermohaline circulation under an ice shelf, *Antarct. Sci.*, *1*(4), 325–336.

Hellmer, H. H., F. Kauker, R. Timmermann, J. Determann, and J. Rae (2012), Twenty-first-century warming of a large Antarctic ice-shelf cavity by a redirected coastal current, *Nature*, *485*, 225–228, doi:10.1038/nature11064.

Holland, D. M., and A. Jenkins (1999), Modeling thermodynamic ice-ocean interactions at the base of an ice shelf, *J. Phys. Oceanogr.*, *29*, 1787–1800.

Holland, D. M., S. S. Jacobs, and A. Jenkins (2003), Modelling the ocean circulation beneath the Ross Ice Shelf, *Antarct. Sci.*, *15* (1), doi:10.1017/S0954102003001019.

Holland, P. R., H. F. J. Corr, D. G. Vaughan, A. Jenkins, and P. Skvarca (2009), Marine ice in Larsen Ice Shelf, *Geophys. Res. Lett.*, *36*, L11,604, doi:10.1029/2009GL038162.

Holland, P. R., A. Jenkins, and D. M. Holland (2010), Ice and ocean processes in the Bellingshausen Sea, Antarctica, *J. Geophys. Res.*, *115*, C05,020, doi:10.1029/2008JC005219.

Hooke, R. L. (2005), *Principles of Glacier Mechanics*, 429 pp., Cambridge University Press, New York.

Horgan, H. J., R. T. Walker, S. Anandakishnan, and R. B. Alley (2011), Surface elevation changes at the front of the Ross Ice Shelf: Implication for basal melting, *J. Geophys. Res.*, *116*, C02,005, doi:10.1029/2010JC006192.

Humbert, A. (2010), The temperature regime of Fimbulisen, Antarctica, *Ann. Glaciol.*, *51*(55), 56–64.

Jacobs, S. S. (2004), Bottom water production and its links with the thermohaline circulation, *Antarct. Sci.*, *16* (4), 427–437, doi:10.1017/S095410200400224X.

Jacobs, S. S., and C. F. Giulivi (2010), Large multidecadal salinity trends near the Pacific-Antarctic continental margin, *J. Climate*, *23*, 4508–4524, doi:10.1175/2010JCLI3284.1.

Jacobs, S. S., H. H. Hellmer, C. S. M. Doake, A. Jenkins, and R. M. Frolich (1992), Melting of ice shelves and the mass balance of Antarctica, *J. Glaciol.*, *38*(130), 375–387.

Jacobs, S. S., H. H. Hellmer, and A. Jenkins (1996), Antarctic ice sheet melting in the Southeast Pacific, *Geophys. Res. Lett.*, *23*(9), 957–960.

Jacobs, S. S., C. F. Giulivi, and P. A. Mele (2002), Freshening of the Ross Sea during the late 20th century, *Science*, *297*, 386–389, doi:10.1126/science.1069574.

Jacobs, S. S., A. Jenkins, C. F. Giulivi, and P. Dutrieux (2011), Stronger ocean circulation and increased melting under Pine Island Glacier ice shelf, *Nat. Geosci.*, *4*, 519–523, doi:10.1038/NGEO1188.

Jenkins, A., and C. S. M. Doake (1991), Ice-ocean interaction on Ronne Ice Shelf, Antarctica, *J. Geophys. Res.*, *96*, 791–813.

Jenkins, A., and D. Holland (2007), Melting of floating ice and sea level rise, *Geophys. Res. Lett.*, *34*, L16,609, doi:10.1029/2007GL030784.

Jenkins, A., and D. M. Holland (2002), A model study of ocean circulation beneath Filchner-Ronne Ice Shelf, Antarctica: Implications for bottom water formation, *Geophys. Res. Lett.*, *29*(8), 1193, doi:10.1029/2001GL014589.

Jenkins, A., and S. Jacobs (2008), Circulation and melting beneath George VI Ice Shelf, Antarctica, *J. Geophys. Res.*, *113*, C04,013, doi:10.1029/2007JC004449.

Jenkins, A., D. G. Vaughan, S. S. Jacobs, H. H. Hellmer, and J. R. Keys (1997), Glaciological and oceanographic evidence of high melt rates beneath Pine Island Glacier, West Antarctica, *J. Glaciol.*, *43*, 114–120.

Joughin, I., and L. Padman (2003), Melting and freezing benearth Filchner-Ronne Ice Shelf, Antarctica, *Geophys. Res. Lett.*, *30*(9), 1477, doi:10.0129/2003GL016941.

Kusahara, K., H. Hasumi, and T. Tamura (2010), Modeling sea ice production and dense shelf water formation in coastal polynyas around East Antarctica, *J. Geophys. Res.*, *115*, C10,006, doi:10.1029/2010JC006133.

Kusahara, K., H. Hasumi, and G. D. Williams (2011), Dense shelf water formation and brine-driven circulation in the Adélie and George V Land region, *Ocean Model.*, *37*, 122–138, doi:10.1016/j.ocemod.2011.01.008.

Leonard, B. P., M. K. MacVean, and A. P. Lock, (1993), Positivity-preserving numerical schemes for multidimensional advection, *Tech. Memo 106005*, 62 pp., NASA.

Levitus, S., J. Antonov, and T. Boyer (2005), Warming of the world ocean, 1955–2003, *Geophys. Res. Lett.*, *32*, L02,604, doi:10.1029/2004GL021592.

Li, X., R. J. Rowley, J. C. Kostelnick, D. Braaten, J. Meisel, and K. Hulbutta (2009), GIS analysis of global impacts from sea level rise, *Photogramm. Eng. Rem. S.*, *75*(7), 807–818.

Lingle, C. S., D. H. Schilling, J. L. Fastook, W. S. B. Patterson, and T. J. Brown (1991), A flow band model of the Ross Ice Shelf, Antarctica: Response to CO_2-induced climatic warming, *J. Geophys. Res.*, *96*, 6849–6871.

Loose, B., P. Schlosser, W. M. Smethie, and S. Jacobs (2009), An optimized estimate of glacial melt from the Ross Ice Shelf using noble gases, stable isotopes, and CFC transient tracers, *J. Geophys. Res.*, *114*, C08,007, doi:10.1029/2008JC005048.

Losch, M. (2008), Modeling ice shelf cavities in a z coordinate ocean general circulation model, *J. Geophys. Res.*, *113*, C08,043, doi:10.1029/2007JC004368.

Makinson, K., P. R. Holland, A. Jenkins, K. W. Nicholls, and D. M. Holland (2011), Influence of tides on melting and freezing beneath Filchner-Ronne Ice Shelf, Antarctica, *Geophys. Res. Lett.*, *38*, L06,601, doi:10.1029/2010GL046462.

Marsland, S. J., N. L. Bindoff, G. D. Williams, and W. F. Budd (2004), Modeling water mass formation in the Mertz Glacier Polynya and Adélie Depression, East Antarctica, *J. Geophys. Res.*, *109*, C11,003, doi:10.1029/2004JC002441.

Morales Maqueda, M. A., A. J. Willmott, and N. R. T. Biggs (2004), Polynya dynamics: A review of observations and modeling, *Rev. Geophys.*, *42*, RG1004, doi:10.1029/2002RG000116.

Mueller, R. D., L. Padman, M. S. Dinniman, S. Y. Erofeeva, H. A. Fricker, and M. A. King (2012), Impact of tide-topography interactions on basal melting of Larsen C Ice Shelf, Antarctica, *J. Geophys. Res.*, *117*, C05,005, doi:10.1029/2011JC007263.

Nicholls, K. W., L. Padman, M. Schröder, R. A. Woodgate, A. Jenkins, and S. Østerhus (2003), Water mass modification over the continental shelf north of Ronne Ice Shelf, Antarctica, *J. Geophys. Res.*, *108*(8), 3260, doi:10.1029/2002JC001713.

Nicholls, K. W., K. Makinson, and S. Østerhus (2004), Circulation and water masses beneath the northern Ronne Ice Shelf, Antarctica, *J. Geophys. Res.*, *109*, C12,017, doi:10.1029/2004JC002302.

Nicholls, K. W., E. P. Abrahamsen, K. J. Heywood, K. Stansfield, and S. Østerhus (2008), High-latitude oceanography using the autosub autonomous underwater vehicle, *Limnol. Oceanogr.*, *53*(5), 2309–2320.

Nicholls, K. W., S. Østerhus, K. Makinson, T. Gammerlsrød, and E. Fahrback (2009), Ice-ocean processes over the continental shelf of the southern Weddell Sea, Antarctica: A review, *Rev. Geophys.*, *47*, 23 pp., doi:10.1029/2007RG000250.

Noh, Y., and H. J. Kim (1999), Simulations of temperature and turbulence structure of the oceanic boundary layer with the improved near-surface process, *J. Geophys. Res.*, *104*(C7), 15,621–15,634.

Ohshima, K. I., T. Takizawa, S. Ushio, and T. Kawamura (1996), Seasonal variations of the Antarctic coastal ocean in the vicinity of Lützow-Holm Bay, *J. Geophys. Res.*, *101*, 20,617–20,628.

Olbers, D., and H. H. Hellmer (2010), A box model of circulation and melting in ice shelf caverns, *Ocean Dynam.*, *60*, 141–153, doi:10.1007/s10236-009-0252-z.

Orsi, A. H., G. C. Johnson, and J. L. Bullister (1999), Circulation, mixing, and production of Antarctic Bottom Water, *Prog. Oceanogr.*, *43*(1), 55–109.

Payne, A. J., P. R. Holland, A. P. Shepherd, I. C. Rutt, A. Jenkins, and I. Joughin (2007), Numerical modeling of ocean-ice interactions under Pine Island Bays ice shelf, *J. Geophys. Res.*, *112*, C10,019, doi:10.1029/2006JC003733.

Pillsbury, R. D., and S. S. Jacobs (1985), Preliminary observations from long-term current meter moorings near the Ross Ice Shelf, Antarctica, *Antarct. Res.*, *43*, 87–107

Potter, J. R., and J. G. Paren (1985), *Interaction Between Ice Shelf and Ocean in George VI Sound, Antarctica, Oceanology of the Antarctic Continental Shelf*, 35–58 pp., Antarc. Res. Ser., vol. 43, AGU, Washington, D.C.

Potter, J. R., J. G. Paren, and J. Loynes (1984), Glaciological and oceanographic calculations of the mass balance and oxygen isotope ratio of a melting ice shelf, *J. Glaciol.*, *30*(105), 161–170.

Pritchard, H. D., R. J. Arthern, D. G. Vaughan, and L. A. Edwards (2009), Extensitve dynamic thinning on the margins of the Greenland and Antarctic ice sheets, *Nature*, *461*, 971–975, doi:10.1038/nature08471.

Pritchard, H. D., S. R. M. Ligtenberg, H. A. Fricker, D. G. Vaughan, M. R. van den Broeke, and L. Padman (2012), Antarctic ice-sheet loss driven by basal melting of ice shelves, *Nature*, *484*, 502–505, doi:10.1038/nature10968.

Reddy, T. E., D. M. Holland, and K. R. Arrigo (2010), Ross ice shelf cavity circulation, residence time, and melting: Results from a model of oceanic chlorofluorocarbons, *Cont. Shelf Res.*, *30*, 733–742, doi:10.1016/j.csr.2010.01.007.

Rignot, E., and S. S. Jacobs (2002), Rapid bottom melting widespread near Antarctic ice sheet grounding lines, *Science*, *296*, 2020–2023.

Rignot, E., and S. S. Jacobs (2008), Ice-shelf melting around Antarctica, American Geophysical Union, Fall Meeting [Abstract C41D-02].

Rignot, E., J. L. Bamber, M. R. van den Broeke, C. Davis, Y. Li, W. J. van de Berg, and E. V. Meijgaard (2008), Recent Antarctic ice mass loss from radar interferometry and regional climate modelling, *Nat. Geosci.*, *1*, 106–110, doi:10.1038/ngeo102.

Rignot, E., I. Velicogna, B. van den M. R., A. Monaghan, and J. T. M. Lenaerts (2011), Acceleration of the contribution of the Greenland and Antarctic ice sheets to sea level rise, *Geophys. Res. Lett.*, *38*, L05,503, doi:10.1029/2011GL046583.

Rignot, E. J. (1998), Fast recession of a West Antarctic glacier, *Science*, *281*, 549–551, doi:10.1126/science.281.5376.549.

Rintoul, S. R. (2007), Rapid freshening of Antarctic Bottom Water formed in the Indian and Pacific oceans, *Geophys. Res. Lett.*, *34*, L06,606, doi:10.1029/2006GL028550.

Röske, F. (2006), A global heat and freshwater forcing dataset for ocean models, *Ocean Model.*, *11*, 235–297, doi:10.1016/j.ocemod.2004.12.005.

Rowley, R. J., J. C. Kostelnick, D. Braaten, X. Li, and J. Meisel (2007), Risk of rising sea level to population and land area, *EOS*, *88* (9), 105–107.

Schlosser, P., R. Bayer, A. Foldvik, T. Gammerlsrød, G. Rohardt, and K. O. Münnich (1990), Oxygen 18 and Helium as tracers of Ice Shelf Water and water/ice interaction in the Weddell Sea, *J. Geophys. Res.*, *95*(C3), 3253–3263.

Schodlok, M. P., D. Menemenlis, E. Rignot, and M. Studinger (2012), Sensitivity of the ice-shelf/ocean system to the sub-ice-shelf cavity shape measured by NASA IceBridge in Pine Island Glacier, West Antarctica, *Ann. Glaciol.*, *53*(60), 156–162, doi:10.3189/2012AoG60A073.

Schoof, C. (2007), Ice sheet grounding line dynamics: Steady states, stability, and hysteresis, *J. Geophys. Res.*, *112*, F03S28, doi:10.1029/2006JF000664.

Shabtaie, S., and C. R. Bentley (1987), West Antarctic ice streams draining into the Ross Ice Shelf: Configuration and mass balance, *J. Geophys. Res.*, *92*, 1311–1336.

Shepherd, A., D. Wingham, and E. Rignot (2004), Warm ocean is eroding West Antarctic Ice Sheet, *Geophys. Res. Lett.*, *31*, L23,402, doi:10.1029/2004GL021106.

Shepherd, A., et al. (2012), A reconciled estimate of ice-sheet mass balance, *Science*, *338*, 1183–1189, doi:10.1126/science.1228102.

Shimada, K., S. Aoki, K. I. Ohshima, and R. Rintoul (2012), Influence of Ross Sea Bottom Water changes on the warming and freshening of the Antarctic Bottom Water in the Australian-Antarctic Basin, *Ocean Sci.*, *8*, 419–432, doi:10.5194/os-8-419-2012.

Smedsrud, L. H., A. Jenkins, D. M. Holland, and O. A. Nost (2006), Modeling ocean processes below Fimbulisen, Antarctica, *J. Geophys. Res.*, *111*, C01,107, doi:10.1029/2005JC002915.

Smethie, W. M., and S. S. Jacobs (2005), Circulation and melting under the Ross Ice Shelf: Estimates from evolving CFC, salinity and temperature fields in the Ross Sea, *Deep-Sea Res.*, *52*, 959–978.

Steele, M., R. Morley, and W. Ermold (2001), PHC: A global ocean hydrography with a high-quality Arctic Ocean, *J. Climate*, *14*, 2079–2087.

Tamura, T., K. I. Ohshima, and S. Nihashi (2008), Mapping of sea ice production for Antarctic coastal polynyas, *Geophys. Res. Lett.*, *35*, L07,606, doi:10.1029/2007GL032903.

Thoma, M., K. Grosfeld, and M. A. Lange (2006), Impact of the Eastern Weddell Ice Shelves on water masses in the eastern Weddell Sea, *J. Geophys. Res.*, *111*, C12,010, doi:10.1029/2005JC003212.

Thoma, M., A. Jenkins, D. Holland, and S. Jacobs (2008), Modelling Circumpolar Deep Water intrusions on the Amundsen Sea continental shelf, Antarctica, *Geophys. Res. Lett.*, *35*, L18,602, doi:10.1029/2008GL034939.

Thoma, M., K. Grosfeld, K. Makinson, and M. A. Lange (2010), Modelling the impact of ocean warming on melting and water masses of ice shelves in the Eastern Weddell Sea, *Ocean Dynam.*, *60*, 480–489, doi:10.1007/s10236-010-0262-x.

Timmermann, R., A. Beckmann, and H. H. Hellmer (2002a), Simulations of ice-ocean dynamics in the Weddell Sea 1. Model configuration and validation, *J. Geophys. Res.*, *107*, C3, 3024, doi:10.1029/2000JC000741.

Timmermann, R., H. H. Hellmer, and A. Beckmann (2002b), Simulations of ice-ocean dynamics in the Weddell Sea 2. Interannual variability 1985–1993, *J. Geophys. Res.*, *107*, C3, 3025, doi:10.1029/2000JC 000742.

Timmermann, R., et al. (2010), A consistent data set of Antarctic ice sheet topography, cavity geometry, and global bathymetry, *Earth Syst. Sci. Data*, *2*, 261–273, doi:10.5194/essd-2-261-2010.

Timmermann, R., Q. Wang, and H. H. Hellmer (2012), Ice-shelf basal melting in a global finite-element sea-ice/ice-shelf/ocean model, *Ann. Glaciol.*, *53*(60), 303–314, doi:10.3189/2012AoG60A156.

Wen, J., Y. Wang, W. Wang, K. C. Jezek, H. Liu, and I. Allison (2010), Basal melting and freezing under the Amery Ice Shelf, East Antarctica, *J. Glaciol.*, *56*(195), 81–90.

Williams, M. J. M., R. C. Warner, and W. F. Budd (1998), The effects of ocean warming on melting and ocean circulation under the Arnery Ice Shelf, East Antarctica, *Ann. Glaciol.*, *27*, 75–80.

Williams, M. J. M., K. Grosfeld, R. C. Warner, R. Gerdes, and J. Determann (2001), Ocean circulation and ice-ocean interaction beneath the Amery Ice Shelf, Antarctica, *J. Geophys. Res.*, *106*, 22,383–22,399.

Williams, M. J. M., R. C. Warner, and W. F. Budd (2002), Sensitivity of the Amery Ice Shelf, Antarctica, to changes in the climate of the Southern Ocean, *J. Climate*, *15*, 2740–2757.

Wingham, D. J., D. W. Wallis, and A. Shepherd (2009), Spatial and temporal evolution of Pine Island Glacier thinning, 1995–2006, *Geophys. Res. Lett.*, *36*, L17,501, doi:10.1029/2009GL039126.

Yin, J., J. T. Overpeck, S. M. Griffies, A. Hu, J. L. Russell, and R. J. Stouffer (2011), Different magnitudes of projected subsurface ocean warming around Greenland and Antarctica, *Nat. Geosci.*, *4*, 524–528, doi:10.1038/NGEO1189.

Yu, J., H. Liu, K. C. Jezek, R. C. Warner, and J. Wen (2010), Analysis of velocity field, mass balance, and basal melt of the Lambert Glacier-Amery Ice Shelf system by incorporating Radarsat SAR interferometry and ICESat laser altimetry measurements, *J. Geophys. Res.*, *115*, B11,102, doi:10.1029/2010JB007456.

Zotikov, I. A., V. S. Zagorodnov, and J. V. Raikovsky (1980), Core drilling through the Ross Ice Shelf (Antarctica) confirmed basal freezing, *Science*, *207*(28), 1463–1465.